



**HAL**  
open science

# Geographical, Seasonal and Diurnal Variations of Acoustic Attenuation, and Sound Speed in the Near-Surface Martian Atmosphere

Martin Gillier, Andi Petculescu, Naomi Murdoch, Alexander E. Stott, Solène Gerier, Sylvestre Maurice, David Mimoun

► **To cite this version:**

Martin Gillier, Andi Petculescu, Naomi Murdoch, Alexander E. Stott, Solène Gerier, et al.. Geographical, Seasonal and Diurnal Variations of Acoustic Attenuation, and Sound Speed in the Near-Surface Martian Atmosphere. *Journal of Geophysical Research: Planets*, 2024, 129, 10.1029/2023JE008257 . insu-04833979

**HAL Id: insu-04833979**

**<https://insu.hal.science/insu-04833979v1>**

Submitted on 12 Dec 2024

**HAL** is a multi-disciplinary open access archive for the deposit and dissemination of scientific research documents, whether they are published or not. The documents may come from teaching and research institutions in France or abroad, or from public or private research centers.

L'archive ouverte pluridisciplinaire **HAL**, est destinée au dépôt et à la diffusion de documents scientifiques de niveau recherche, publiés ou non, émanant des établissements d'enseignement et de recherche français ou étrangers, des laboratoires publics ou privés.



Distributed under a Creative Commons Attribution 4.0 International License

## Geographical, Seasonal and Diurnal Variations of Acoustic Attenuation, and Sound Speed in the Near-Surface Martian Atmosphere


**Key Points:**

- Attenuation and speed of sound are modeled at every point of the Martian surface
- Sound attenuation and speed are most affected by the variation of pressure and temperature associated with the diurnal and seasonal cycles
- The variations of sound attenuation and speed during a given day are very strong compared to Earth

**Correspondence to:**








M. Gillier,  
[martin.gillier@isae-supaero.fr](mailto:martin.gillier@isae-supaero.fr)

**Citation:**

Gillier, M., Petculescu, A., Murdoch, N., Stott, A. E., Gerier, S., Maurice, S., & Mimoun, D. (2024). Geographical, seasonal and diurnal variations of acoustic attenuation, and sound speed in the near-surface Martian atmosphere. *Journal of Geophysical Research: Planets*, 129, e2023JE008257. <https://doi.org/10.1029/2023JE008257>

Received 18 DEC 2023

Accepted 22 APR 2024

Martin Gillier<sup>1</sup> , Andi Petculescu<sup>2</sup> , Naomi Murdoch<sup>1</sup> , Alexander E. Stott<sup>1</sup> , Solène Gerier<sup>1</sup> , Sylvestre Maurice<sup>3</sup> , and David Mimoun<sup>1</sup> 

<sup>1</sup>Institut Supérieur de l'Aéronautique et de l'Espace (ISAE-SUPAERO), Université de Toulouse, Toulouse, France,

<sup>2</sup>Department of Physics, University of Louisiana at Lafayette, Lafayette, LA, USA, <sup>3</sup>CNRS, CNES, Institut de Recherche en Astrophysique et Planétologie (IRAP), Université de Toulouse 3 Paul Sabatier, Toulouse, France

**Abstract** This work introduces a comprehensive model of sound attenuation and speed on Mars, in light of the recent operation of several microphones on the surface of Mars. The proposed acoustic model calculates the sound speed and attenuation throughout the near-surface Martian atmosphere based on first-principles. We evaluate the effects of the seasonal and diurnal cycle of air temperature, pressure and CO<sub>2</sub>, as well as the concentration of airborne dust on the sound attenuation. The attenuation and speed of sound are most sensitive to the air temperature and, therefore, they vary with the diurnal temperature cycle and to a lesser degree with the seasonal changes in temperature. The speed of sound also varies with the seasonal variations of the concentration of CO<sub>2</sub>. The main outcome of this work is an acoustic model capable of computing the sound speed and attenuation for any location at the Martian surface at any time of year and any time of day.

**Plain Language Summary** Sound offers new means of investigating the Martian environment. To study the properties of sound sources on Mars, or to derive atmospheric properties from the way sound travels in the Martian atmosphere, a model of the sound attenuation and speed on Mars is needed. In this paper, we propose such a model that allows the sound attenuation and speed at the Martian surface to be computed at any point and time. We investigate how these two properties change with air temperature, pressure, the chemical composition of the Martian atmosphere, the concentration of airborne dust, and with time of day and season. This paints the picture of Mars as a very contrasting planet acoustically, with a very wide range of attenuation and speed of sound compared to Earth because of the daily variations of temperature and the yearly variations of pressure and chemical composition.

### 1. Introduction

Acoustics has become a reliable tool for investigating atmospheric properties, owing to the intrinsic coupling between sound and its propagation medium. Based on many decades of successful application of acoustic techniques to study Earth's atmosphere, the scientific community has now deployed acoustic sensors to other planetary atmospheres. Earlier studies have highlighted the interest of acoustics for planetary exploration (Leighton & Petculescu, 2008) with application ranging from sonar (Ainslie & Leighton, 2016) to probing of outer planet atmospheres vertical structure (R. D. Lorenz, 1998). Microphones have recorded wind-induced noise on the surface of Venus during the Soviet missions Venera 13 and 14 (Ksanfomaliti et al., 1982). The Huygens probe that landed on Titan carried several acoustic instruments, including a sonar (Towner et al., 2006) and a speed of sound sensor (Hagermann et al., 2007). Mars Polar Lander (1999) and Phoenix (2008) both carried microphones that were either lost along with the probes or not turned on due to instrument safety concerns. More recently, several microphones have landed and operated on Mars, namely the Entry, Descent, and Landing and the SuperCam microphones on the NASA Perseverance rover (Maurice et al., 2022; Mimoun et al., 2023) and the Chinese National Space Administration Zhurong rover microphone (Zou et al., 2021). These microphones have already yielded results on the acoustic properties of the Martian atmosphere, either by listening to artificial sound sources such as the Ingenuity helicopter (R. D. Lorenz et al., 2023) and the laser-induced breakdown spectroscopy (LIBS) experiment (Chide et al., 2022), or by recording the signals induced by the Martian environment such as the wind (Stott et al., 2023) and a dust devil (Murdoch et al., 2022).

© 2024. The Authors.

This is an open access article under the terms of the [Creative Commons Attribution License](https://creativecommons.org/licenses/by/4.0/), which permits use, distribution and reproduction in any medium, provided the original work is properly cited.

In this context, a model of sound propagation at the Martian surface is needed. Indeed, to know the acoustic properties of a sound source from the received signal, one needs to account for the effects of sound propagation in the atmosphere. Conversely, if the source is known, the received signal can be used to study the properties of the propagation medium. In both cases, the knowledge of the link between the atmosphere's properties and the way an acoustic wave travels through it is required. A sound propagation model can also be used to define the requirements of future acoustic instruments and experiments based on the characteristics of the sound source it is intended to record.

The design of the SuperCam microphone (Mimoun et al., 2023) was based on the use of existing models of the propagation of sound in the Martian atmosphere in H. E. Bass and Chambers (2001), Williams (2001) and Petculescu and Lueptow (2007). These models allowed an attenuation coefficient and a speed of sound to be computed for a general Martian atmosphere or for a profile from the surface to the top of the atmosphere.

In this work, we propose a model to quantify the attenuation coefficient and the speed of sound at a given time and location on the Martian surface as a first step to a more complete acoustic propagation model. The discussion is focused on the near-surface, that is, the first 20 m of the Martian atmosphere, as the goal is to understand the acoustic environment in which landers, rovers, drones and any future human exploration would operate. The method we use, described in Section 2, consists first in taking outputs of the Martian Climate Database (MCD, see Forget et al. (1999) and Millour et al. (2018)) to get all the relevant properties of the Martian atmosphere at the place and time of interest (Section 2.1). A physics-based acoustic model (PBAM) (Dain & Lueptow, 2001; Petculescu & Lueptow, 2007) is then used to determine the attenuation coefficient and the speed of sound for a dry atmosphere at each point of the propagation space from the MCD output (Section 2.4). A model of suspension acoustics is used to take into account the presence of airborne dust (Section 2.5). This is the first time that attenuation and speed of sound at the Martian surface are computed with such a fine spatio-temporal granularity. Based on this model, we are able to investigate the effects of airborne dust concentration (Section 3.1), in addition to the temperature, pressure and chemical composition of the air (Section 3.3). This model allows us to study the influence of longitude and latitude (Section 3.4), season (Section 3.5), time of day (Section 3.6) and altitude (Section 3.7) on the sound attenuation and speed.

## 2. Method

The method presented here allows for the computation of the acoustic attenuation coefficient and the speed of sound at any point of the Martian surface at any time. First, the pressure, temperature, and chemical composition of the location and time of interest are retrieved from the MCD. Then the attenuation coefficient  $\alpha$  is computed as the sum of the classical attenuation coefficient ( $\alpha_{class}$ , see Section 2.3) and the non-classical attenuation coefficient ( $\alpha_{non-class}$ , see Section 2.4). If needed,  $\alpha_{dust}$  (Section 2.5) can be added to  $\alpha$  to represent the case of a dust-loaded atmosphere. The speed of sound is derived from the real part of the effective wavenumber (see Section 2.4).

### 2.1. Martian Atmospheric Parameterization: The Martian Climate Database

We study the propagation of sound under different Martian atmospheric conditions. We focus only on the first tens of meters of the atmosphere, as this is the place where most of the relevant sound detectors (embedded on landers, rovers, and drones) would be operated.

To obtain mean values for all atmospheric parameters, we used the MCD (see Forget et al. (1999) and Millour et al. (2018)). The MCD is a database of meteorological fields derived from numerical simulations of the Martian atmosphere and validated using available observational data. It consists of a 3D grid of  $5.625^\circ$  of longitude and  $3.75^\circ$  of latitude, which corresponds to  $330 \times 450$  km at the surface. There are 73 vertical levels (defined in intervals of pressure), the first one corresponding to 5 m above the surface. Data are available at 12 local times of day for each of the 12 Martian months.

Pressure, temperature, wind velocity, chemical composition and other variables can be determined at any given latitude, longitude, altitude, time of year (expressed as a solar longitude,  $L_s$ ) and time of day (expressed as a Local True Solar Time, LTST) by interpolating between the MCD database values. The horizontal wind velocity and the temperature under the lowest layer (i.e., below 5 m) are computed using the Monin-Obukhov similarity theory.

**Table 1**  
*The Standard Martian Atmosphere Used in This Paper*

Molecule	Molar fraction (%)
CO <sub>2</sub>	96
N <sub>2</sub>	1.89
Ar	1.93
O <sub>2</sub>	0.145
H <sub>2</sub> O	0

*Note.* The values shown in this table were retrieved by the Curiosity rover (Mahaffy et al., 2013) and are used as the default chemical composition.

In this work, when a time and location are specified, atmospheric data from the MCD are used. If time and location are not specified, pressure and temperature are specified and the composition of the Martian atmosphere used is the standard one described in Table 1. Note that only dry atmospheres are considered, so in any case the molar fraction of H<sub>2</sub>O is equal to zero (see Section 4.2 for a discussion on this choice).

## 2.2. Sound Waves and Acoustic Attenuation

This section describes the pressure fluctuations that constitute a sound wave, the attenuation of sound with distance, and introduces the different ways of computing this attenuation. In a spherical harmonic wave of angular frequency  $\omega$ , the sound pressure fluctuations  $p$  are described by Pierce (2019):

$$p(r,t) = \frac{A_0}{r} \exp[i(kr - \omega t)] \quad (1)$$

where  $k$  is the wavenumber,  $A_0$  is a calibration constant expressed in terms of the pressure received at a reference distance and  $r$  is the distance to the source. They exhibit spherical (or geometrical) spreading, decaying with distance even in the absence of intrinsic loss mechanisms. This geometrical spreading is expressed by the  $\frac{1}{r}$  factor.

In general, acoustic propagation is accompanied by intrinsic energy losses. It is customary to express the sound speed and the attenuation through the real and imaginary parts of the complex wavenumber that is,  $k = k_0 + i\alpha$ , where  $k_0 \equiv \omega/c$ ,  $\omega = 2\pi f$  is the angular frequency,  $c$  the speed of sound, and  $\alpha$  the attenuation coefficient.

The attenuation coefficient is usually expressed in m<sup>-1</sup> or dB/km, the latter being typically used in long-range atmospheric studies. This coefficient is approximated as the sum of all the individual contributions from various loss mechanisms.

The attenuation mechanisms can be divided into two main classes: classical and non-classical. Classical attenuation arises from viscosity, thermal conduction, and diffusion (the latter being generally much weaker than the first two). Section 2.3 describes the way classical attenuation is computed in this study. The non-classical attenuation is related to the inability of the molecular internal degrees of freedom (e.g., vibration and rotation) to follow the acoustic temperature oscillations. Section 2.4 describes the way non-classical attenuation as well as speed of sound is computed in this study.

## 2.3. Classical Attenuation

Classical attenuation arises from viscosity, thermal conduction and diffusion. The contribution of the viscosity to acoustic losses is obtained by taking into account the shear viscous forces in the Navier-Stokes equation (Kinsler, 2000), yielding the associated attenuation coefficient:

$$\alpha_v = \frac{8}{3} \frac{\pi^2 f^2}{\rho c^3} \eta \quad (2)$$

with  $f$  the frequency of the sound wave,  $\rho$  the gas mixture density,  $c$  the speed of sound in the gas mixture and  $\eta$  its coefficient of shear viscosity.

During the passage of the acoustic wave, the instantaneous temperature goes through maxima and minima, corresponding, respectively, to compression and rarefaction of the gas. These temperature differences induce irreversible heat transfer, leading to acoustic energy losses. The attenuation coefficient associated with these losses is given (Kinsler, 2000):

$$\alpha_t = (\gamma - 1) \frac{4\pi^2 f^2 K}{\rho c^3 c_p} \quad (3)$$

where  $f$  is the frequency of the sound wave,  $\rho$  the gas mixture density,  $c$  the speed of sound in the gas mixture,  $\gamma$  the heat capacity ratio,  $c_p$  the specific heat at constant pressure and  $K$  the thermal conductivity.

Because of the very high molar fraction of  $\text{CO}_2$ , the contribution from mass diffusion to the overall attenuation is negligible (H. E. Bass & Chambers, 2001) compared to the viscous and conduction losses. Hence, in this work we have:

$$\alpha_{diff} = 0. \quad (4)$$

The specific heat, density, and coefficients of shear viscosity and thermal conductivity depend on the gas composition; in addition, the specific heat vary with temperature and, to a lesser degree, pressure. To compute them, we first retrieved their values for each gas constituting the Martian atmosphere at the relevant pressure and temperature from the NIST chemistry WebBook (Linstrom & Mallard, 2023). Then, the appropriate mixing rules were used to compute these values for the gas mixture. Thus, the molecular weight and specific heat are obtained as simple weighted sums with the corresponding fractions of the species forming the mixture and the Wilke formulae (Poling et al., 2000) are used for viscosity and thermal conductivity.

The classical attenuation coefficient used in this work is then:

$$\alpha_{class} = \alpha_v + \alpha_t \quad (5)$$

#### 2.4. Non-Classical Attenuation and Speed of Sound

The non-classical attenuation occurs in polyatomic molecules whose vibrational and rotational states can affect the overall energy balance through molecular relaxation processes. At a molecular level, there are energy transfers between translational energy on one hand and rotational and vibrational energies on the other hand. However, these exchanges are not as fast as the translational energy variations. This delay in the energy transfer, associated with relaxation times, is responsible for acoustic energy losses.

Several approaches exist to model the vibrational attenuation. For example, Williams (2001) considered that the vibrational attenuation is small when the length of the cycle is too short or too long compared to the relaxation time. As a result, they choose to model it by a parabolic equation whose parameters were defined from experimental data. Molecular vibration can be expressed as the sum of different normal modes, each associated with a wavenumber,  $\nu_i$ . In H. E. Bass and Chambers (2001) only the main vibration mode of  $\text{CO}_2$ , the bending mode ( $\nu_2 = 66,700 \text{ m}^{-1}$ ), was considered, and its effect was computed using the experimentally determined rate of collisions between the different species constituting the Martian atmosphere.

These empirical and semi-empirical models provide a straightforward way to compute the molecular attenuation. However, in order to better test and interpret recorded data in terms of the underlying physics, we derive a first principles model.

The acoustic model used in this work, which will be referred to as the PBAM, is based on work from Dain and Lueptow (2001) and Petculescu and Lueptow (2005). The main idea of this model is to compute an effective wavenumber of a sound wave traveling in a certain gas mixture, that is, a wavenumber that takes into account the internal degrees of freedom created by molecular vibrations. To do so, it is necessary to compute effective specific heat, that is, specific heat that take into account the internal temperatures associated with molecular vibration. This in turn requires the knowledge of various relaxation times associated with the vibrational processes that can be computed from the intermolecular interactions between the different molecules making the gas mixture.

A detailed step-by-step description of this model is available in Appendix A, and some limitations of the model are discussed in Section 4.2. To summarize, this model allows the computation of an effective wavenumber  $k_{eff}$  from a specific gas composition, pressure and temperature. As explained in Section 2.2 this complex wavenumber can be written as:

$$k_{eff}(f) = \frac{2\pi f}{c} + i\alpha_{vib} \quad (6)$$

with  $\alpha_{vib}$  the attenuation coefficient associated with vibrational attenuation, and thus allows the derivation of the vibrational attenuation and the speed of sound.

With a few exceptions (light molecules such as  $H_2$ , very high frequencies, tenuous environments, compressible flows etc.), molecular rotation is in near-equilibrium with translation for many species, hence its contribution to attenuation is negligible and in this work  $\alpha_{rot} = 0$ .

Thus, the non-classical attenuation coefficient is

$$\alpha_{non-class} = \alpha_{vib} \quad (7)$$

The attenuation coefficient of air  $\alpha$  is then obtained as:

$$\alpha = \alpha_{class} + \alpha_{non-class} \quad (8)$$

### 2.5. Attenuation Caused by Airborne Dust

One of the important characteristics of the Martian atmosphere is the presence of dust in suspension. It is known that on Earth particles in suspension can cause attenuation of sound, though in most cases it can be neglected (Henley & Hoidale, 1973). To model the effect of suspended dust on the sound propagation, we used the approach proposed in Temkin (2005) for dilute aerosol suspensions. Using a two phase model, the following dispersion relation (Temkin, 2005) is derived:

$$k_{dust}^2(\omega) = \frac{\omega^2}{c_{Tf}^2} \left( 1 + \frac{\phi_v/\delta}{1 - i\omega\tau_d} \right) \quad (9)$$

with  $\omega$  the angular frequency,  $c_{Tf}$  the isothermal speed of sound,  $\phi_v$  the volume concentration of the particles that is, the ratio between the volume occupied by particles in the suspension and the total volume,  $\delta$  the fluid to particle density ratio and  $\tau_d$  the dynamical relaxation time for the particle,  $\tau_d = \frac{2a^2}{9\nu_f\delta}$  with  $a$  the particle radius and  $\nu_f$  the fluid kinematic viscosity. As explained in Section 2.2 the complex wavenumber  $k_{dust}$  contains both the frequency-dependent speed of sound and attenuation coefficient. Thus, an attenuation coefficient modeling the additional acoustic attenuation caused by dust  $\alpha_{dust}$ , can be computed as the imaginary part of  $k_{dust}$ .

To summarize this section, the attenuation coefficient of air  $\alpha$  is obtained as the sum of the classical and non-classical attenuation, with the possibility to add another coefficient  $\alpha_{dust}$  in the presence of atmospheric dust. The speed of sound at each frequency is given by the real part of the effective wavenumber as shown in Equation 6.

## 3. Results

In this section, the variation of the attenuation coefficient and the speed of sound with different parameters is studied. In particular, we examine the effect of airborne dust concentration (Section 3.1), temperature, pressure and chemical composition of the air (Section 3.3), season (Section 3.5), and time of day (Section 3.6). These parameters are considered in the first 20 m of the Martian atmosphere as this is where most of the relevant sound detectors (embedded on landers, rovers, and drones) would be located. We then show how these parameters impact sound propagation as a function of geographical location and altitude (Sections 3.4 and 3.7).

After showing the attenuation coefficient and the speed of sound for a wide range of frequencies in Section 3.2 we focus on a few frequencies, namely 10, 100, 1,000, and 10,000 Hz, in order to demonstrate the frequency dependence of certain effects. When it is not convenient to show too many frequencies, we focus on 100 Hz as it is representative of the sound produced by Ingenuity, the helicopter traveling along Perseverance rover (R. D. Lorenz et al., 2023), which produces sound at its blade passage frequency (84 Hz) and at its first harmonic (168 Hz). Similarly, after showing the attenuation coefficient and the speed of sound at every point of the Martian surface in Section 3.4 we have chosen to focus on a few locations and especially Perseverance site. When seasonal effects are not studied, we decided to study the Martian atmosphere at  $L_s = 180^\circ$ , the Northern Hemisphere equinox, as it is a time of year when the seasonal effects are not extreme.



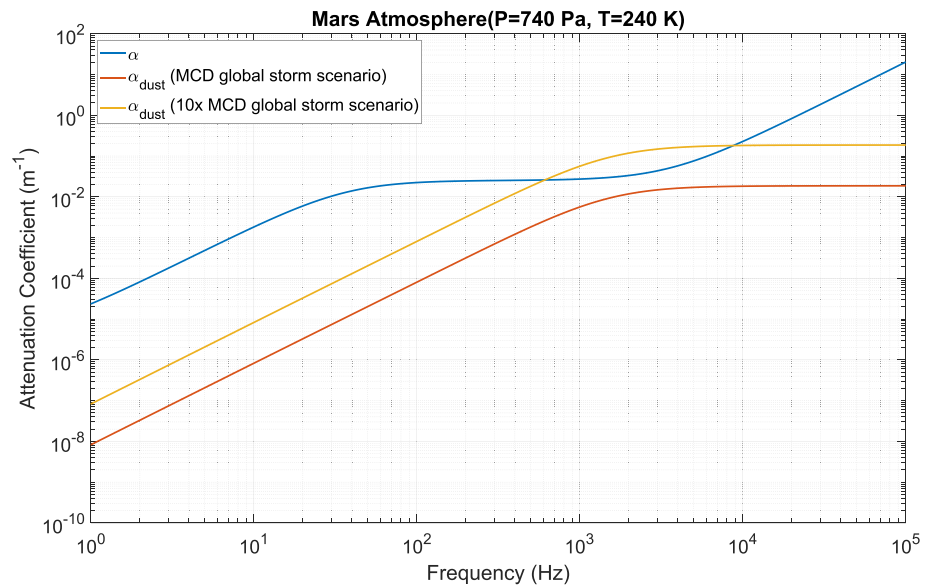


**Figure 1.** Comparison of the air acoustic attenuation ( $\alpha$  see Equation 8) and dust induced attenuation ( $\alpha_{dust}$  see Equation 9). The dust mass mixing ratio is equal to  $1 \times 10^{-3}$  in the Martian Climate Database (MCD) global storm scenario and  $1 \times 10^{-2}$  in the 10x MCD global storm scenario. The atmosphere used is the standard Martian atmosphere (see Table 1) with a temperature of 240 K and a pressure of 740 Pa.

The following results are not exhaustive, as this model can be used to study attenuation and speed of sound in a wide variety of context, but they explore the main parameters to which it is sensitive.

### 3.1. Effect of Airborne Dust

Dust concentration in the Martian atmosphere follows an annual cycle (Liu et al., 2003), with a non-dusty season ( $L_s \sim 0^\circ\text{--}135^\circ$ ) and a dusty one ( $L_s \sim 135^\circ\text{--}360^\circ$ ). Dust that is lifted from the Martian surface through different processes (Kahre et al., 2017) produces dust clouds that can range from a scale of a few meters and a timescale of a few hours to a planetary scale and a timescale of several months. In the latter case, these events are referred to as global dust storms. Large dust storms occur exclusively during the dusty season (Wang & Richardson, 2015). The MCD gives an annual maximum mass mixing ratio of  $1 \times 10^{-3}$  and an air density of  $2.2 \times 10^{-2} \text{ kg/m}^3$  for the global dust storm scenario. These are the values we have used, as they represent a maximum of the dust concentration at the Martian surface. Using a particle radius of  $1.5 \mu\text{m}$  (Kahre et al., 2017), and assuming dust is made of feldspar (Hamilton et al., 2005) that has a density of  $2.56 \times 10^3 \text{ kg/m}^3$  results in a volume concentration of the particles,  $\phi_v$ , of  $9 \times 10^{-9}$ . Figure 1 presents the attenuation induced by suspended dust using a particle radius of  $1.5 \mu\text{m}$  and a mass mixing ratio of  $1 \times 10^{-3}$ .

The attenuation coefficient created by airborne dust is 300 times lower than the dust-free attenuation at 100 Hz and 10 times smaller at 10 kHz. Figure 1 shows that in order for the dust-induced attenuation to have the same order of magnitude as the air-induced attenuation, the dust concentration would need to be 10 times higher than the maximal one given by the MCD for the global storm scenario. This indicates that the attenuation caused by airborne dust near the Martian surface can be safely neglected. Thus, in the following sections, we do not include an attenuation due to dust.

As explained in Section 2.5 there is also an effect of dust on the dispersion of the speed of sound of less than 0.02 m/s between the low and the high frequencies. This is negligible compared to the variations in the sound speed caused by the turbulent fluctuations of the atmosphere, which is typically of 2–3 m/s (Maurice et al., 2022).

### 3.2. Attenuation Coefficient for the Standard Mars Atmosphere

Figure 2 presents the attenuation computed for Mars and Earth surface conditions. The atmospheric composition used for Mars is the standard atmosphere described in Table 1 at 740 Pa and 240 K. For Earth the attenuation is computed at a pressure of 1 atm and 293 K with 20% of relative humidity using the model of H. Bass et al. (1984).

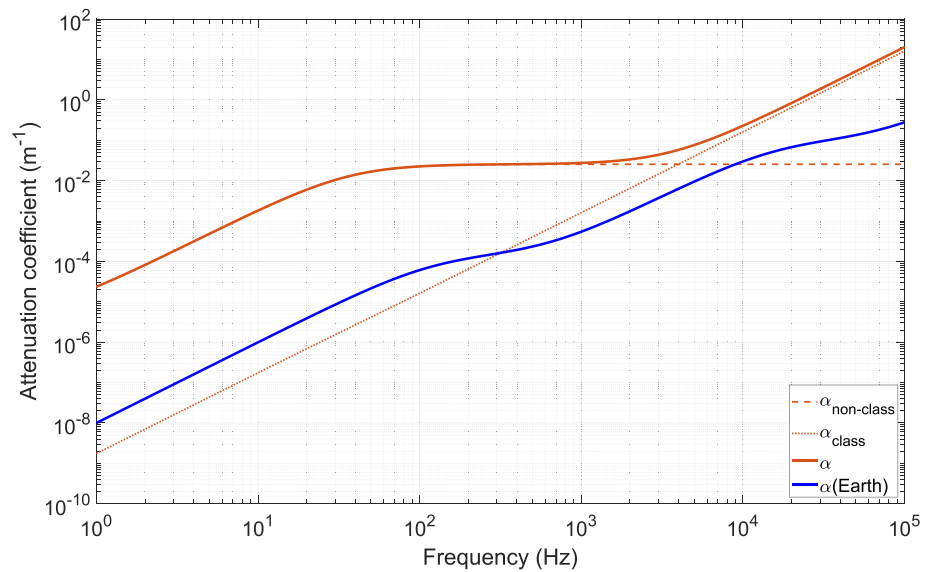


**Figure 2.** Classical and relaxational acoustic attenuation coefficients computed by the physics-based acoustic model for Mars. The atmosphere used is the standard atmosphere described in Table 1 with  $P = 740$  Pa and  $T = 240$  K. For Earth the attenuation is computed at 1 atm and 293 K with 20% of relative humidity (H. Bass et al., 1984).

Figure 2 shows that the relaxational (non-classical) attenuation dominates under 8 kHz with a relaxation frequency (corresponding to the inflexion point) around 50 Hz, while classical attenuation dominates at high frequencies. Earth attenuation is 500 times smaller at low frequencies and 10 times smaller at high frequencies. To that end, sound does not propagate as effectively on Mars as it does on Earth.

Figure 3 presents a comparison of the attenuation models from H. E. Bass and Chambers (2001) and Williams (2001) and the proposed PBAM computed for Martian surface conditions and the standard Martian atmosphere defined in Table 1. The PBAM outputs are in general agreement with those of the Bass-Chambers (less than 20% of difference) and, to a lesser degree, the Williams model. This can be explained by the fact that while the Bass-Chambers and Williams models are empirical, the PBAM developed here is based mostly on first-principles. An interesting characteristic of the PBAM compared to the two other is the additional attenuation in the infrasonic range (below 10 Hz). This attenuation originates from the  $\nu_1$  and  $\nu_3$  relaxation modes of  $\text{CO}_2$  (see Appendix A) which are not considered in the Bass and Chambers or Williams model.

### 3.3. Sensitivity of the Attenuation Coefficient and the Speed of Sound to Temperature, Pressure, and Chemical Composition

#### 3.3.1. Attenuation Coefficient

Figure 4 presents the variation of the attenuation coefficient for a range of temperatures (Figure 4a) and pressures (Figure 4b) typical of the Martian surface, that is, for the range of pressure and temperature that a lander located at a mid-altitude and mid-latitude could experience in a Martian year. These figures show that the attenuation is more sensitive to ambient temperature than to the ambient pressure, most notably between 100 Hz and 10 kHz. Another interesting result is that the amplitude and the direction of the variation in attenuation depend on the frequency range. For example, the attenuation coefficient varies the most between 300 Hz and 3 kHz where the attenuation coefficient increases with increasing temperature, ranging from  $0.04 \text{ m}^{-1}$  for a temperature of 200 K to  $0.3 \text{ m}^{-1}$  for a temperature of 300 K. On the contrary, for frequencies in the 5–100 Hz range, the attenuation coefficient decreases with increasing temperature.

The attenuation coefficient depends on atmospheric composition through the thermophysical and transport parameters, as well as the relaxation times. Using an atmosphere only made of  $\text{CO}_2$  leads to an attenuation coefficient approximately 20% lower for the low frequencies and 30% higher for the high frequencies. The effect of the other gases is thus small, but not negligible. The chemical composition of the lower Martian atmosphere is relatively constant at a given location and any fluctuations do not have a perceptible impact on the attenuation



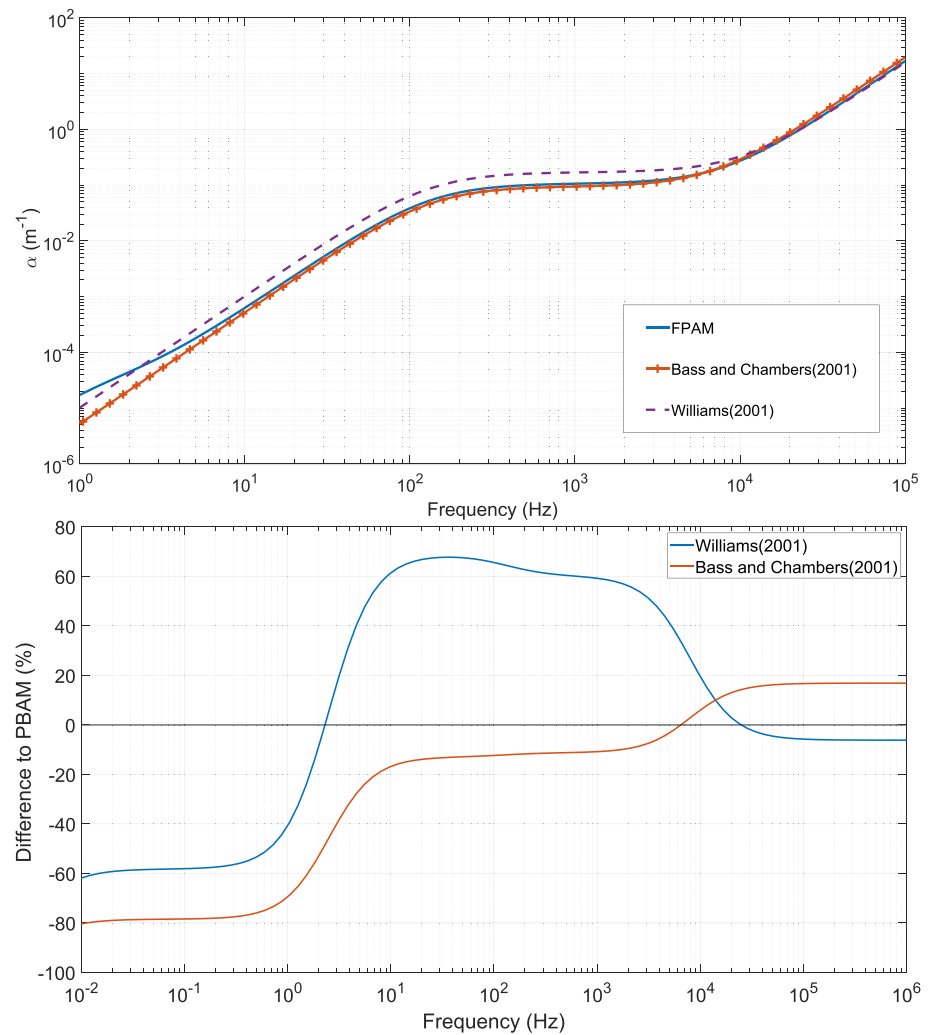


**Figure 3.** Acoustic attenuation of the physics-based acoustic model compared to the one of Williams (2001) and H. E. Bass and Chambers (2001). The atmosphere used is the standard atmosphere described in Table 1 with  $P = 740$  Pa and  $T = 240$  K.

coefficient, except near the poles where the molar fraction of  $\text{CO}_2$  exhibits strong seasonal variations. To summarize, the attenuation coefficient in the Martian atmosphere is mainly a function of temperature and, to a second order, of pressure.

### 3.3.2. Speed of Sound

Molecular vibrational relaxation of the  $\text{CO}_2$  leads to dispersion, that is, a frequency-dependent speed of sound. As shown in Section 2.4, the PBAM provides a way to predict this speed of sound.

Figure 5 presents the speed of sound predicted by the PBAM for a typical range of air temperatures at the Martian surface, that is, between 200 and 300 K. The low-frequency (under 100 Hz) speed of sound ranges between 228 and 272 m/s, and the high frequency one between 235 and 285 m/s.

The variation in the value of speed of sound with pressure is less than 0.01 m/s at high and low frequencies, and so it does not have as large an impact as temperature. The only effect of a change in pressure is to shift the relaxation frequency. The amplitude of this shift when going from 590 to 800 Pa is around 30 Hz.

The speed of sound is sensitive to variations of the chemical composition of the Martian atmosphere. This is demonstrated in Figure 6, which presents the variation of the speed of sound when the molar fraction of  $\text{CO}_2$ ,  $X_{\text{CO}_2}$  is modified (see Table 1). The effect of the molar fraction of  $\text{CO}_2$  is evaluated by varying the chemical

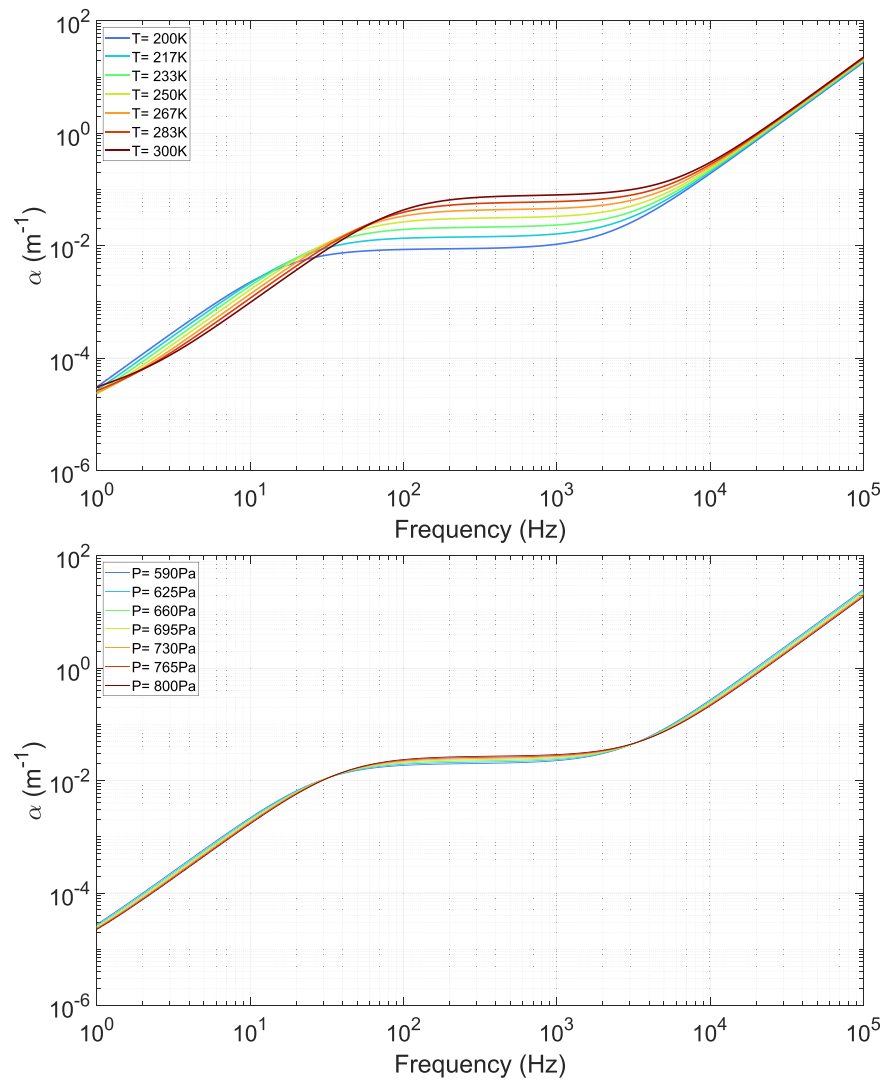


**Figure 4.** Sensitivity of the attenuation coefficient to a range of atmospheric temperatures (top) and pressures (bottom) typical at the Martian surface.  $P = 740$  Pa in the top figure and  $T = 240$  K in the bottom one.

composition of the gas mixture used as an input of the PBAM. The molar fraction of  $N_2$  is also adjusted accordingly. In these figures, the speed of sound is computed at a temperature of 240 K and a pressure of 740 Pa.

Figure 6 shows that every one percent of decrease in the molar fraction of  $CO_2$  leads to an increase in the speed of sound of  $\sim 0.6$  m/s. This means that a speed of sound sensor with a sensitivity of 0.06 m/s would be capable to detect a variation in the  $CO_2$  molar fraction at a level of 1 part in 1,000, as was suggested in R. Lorenz (2000). Note that when Ar replaces the missing  $CO_2$  instead of  $N_2$  the increase in the speed of sound is greater. Thus, if the molar fraction of  $CO_2$  and the temperature is known, one could infer the relative proportion of Ar and  $N_2$  from a speed of sound measurement. One must keep in mind that such a wide range of  $CO_2$  molar fraction is only experienced close to the poles because of the  $CO_2$  yearly cycle (see Section 3.5).

In summary, the speed of sound is frequency dependent and increases with temperature and, to a lesser degree, with the decrease of  $CO_2$  molar fraction. It must be noted that here we are discussing the speed of sound in an stationary medium, the effective speed of sound would be different in the presence of wind.

To conclude this section Figure 7 shows the variations of the relaxation frequency of the attenuation coefficient and speed of sound with temperature, pressure and the molar fraction of  $CO_2$ .

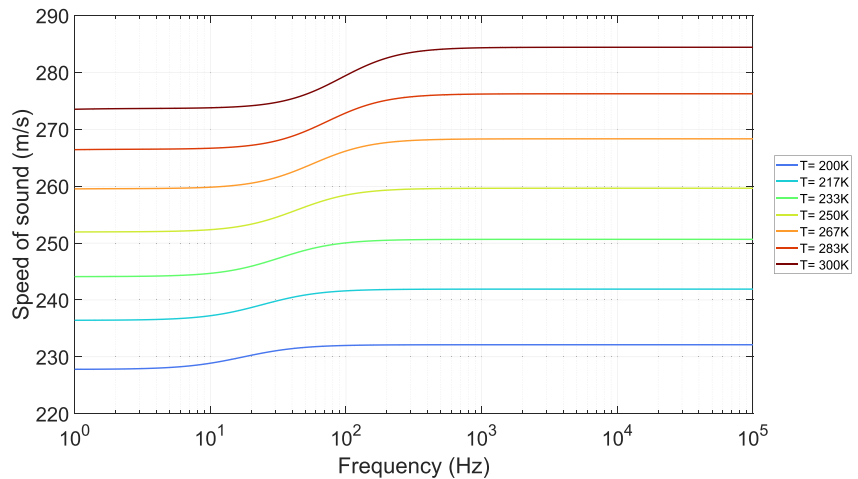


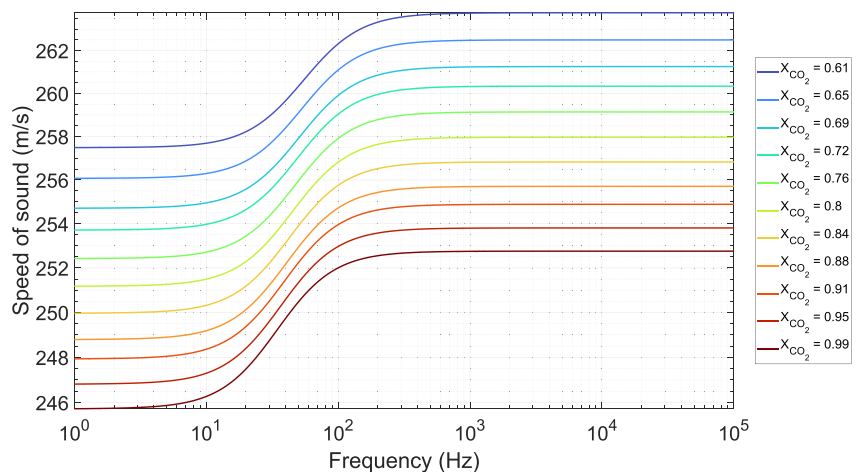
**Figure 5.** Speed of sound on the Martian surface as predicted by the physics-based acoustic model for a range of temperatures typical of the Martian surface.

### 3.4. Attenuation Coefficient and the Speed of Sound Across the Martian Surface

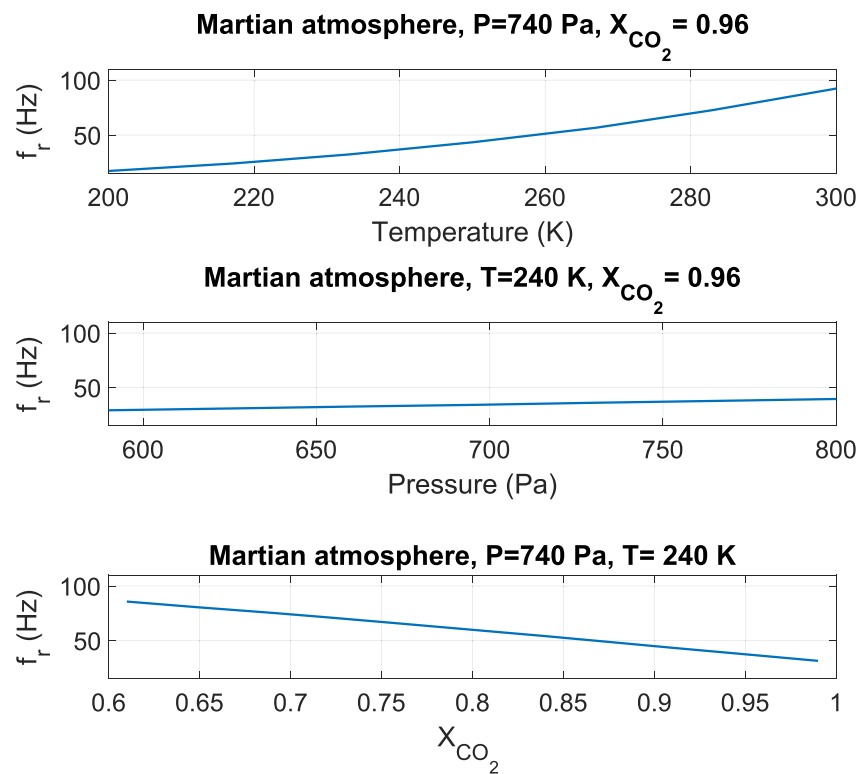
In this section, we introduce several maps of the Martian surface to demonstrate the range of attenuation and speed of sound across the planet. The mapped attenuation and sound speed values are obtained based on the outputs of the MCD at  $L_s = 180^\circ$  (northern autumn equinox) at 12 Universal Martian Solar Time (UMST) i.e. solar time at a longitude of 0) 3 m above the ground. This means that the Sun nadir is at a longitude and a latitude of 0.

Figure 8 shows the map of the temperature with some geographical features of Mars annotated for context. The Perseverance site ( $18.45^\circ\text{N}$ ,  $77.4^\circ\text{E}$ ) and an arbitrarily chosen point at high latitude ( $85^\circ\text{N}$ ,  $0^\circ\text{E}$ ) are indicated, as we will focus on these later in Section 3. Some of the highest points of Mars (Olympus Mons and Elysium Mons) as well as some depressions (Valles Marineris, Hellas Planitia and Argyre Planitia) are also indicated to give a sense of the relief.

The temperature is higher at low latitudes, and lower near the South Pole than near the North Pole because of the higher altitude of the southern plateau. Temperatures are also higher between an East longitude of  $-90$  and  $90^\circ$ , as they are in daylight at the time of the simulation.



**Figure 6.** Speed of sound on the Martian surface as predicted by the physics-based acoustic model for  $\text{CO}_2$  molar fraction ( $X_{\text{CO}_2}$ ) ranging from the minimum to the maximum that is expected at the Martian surface according to the Martian Climate Database. Speed of sound is computed at a temperature of 240 K and a pressure of 740 Pa.



**Figure 7.** Relaxation frequency of the attenuation coefficient and speed of sound predicted by the physics-based acoustic model. Top: variations of the relaxation frequency with temperature in a Martian atmosphere with a pressure of 740 Pa and a molar fraction of CO<sub>2</sub> of 0.96. Middle: variations of the relaxation frequency with pressure in a Martian atmosphere with a temperature of 240 Pa and a molar fraction of CO<sub>2</sub> of 0.96. Bottom: variations of the relaxation frequency with molar fraction of CO<sub>2</sub> in a Martian atmosphere with a pressure of 740 Pa and a temperature of 240 K.

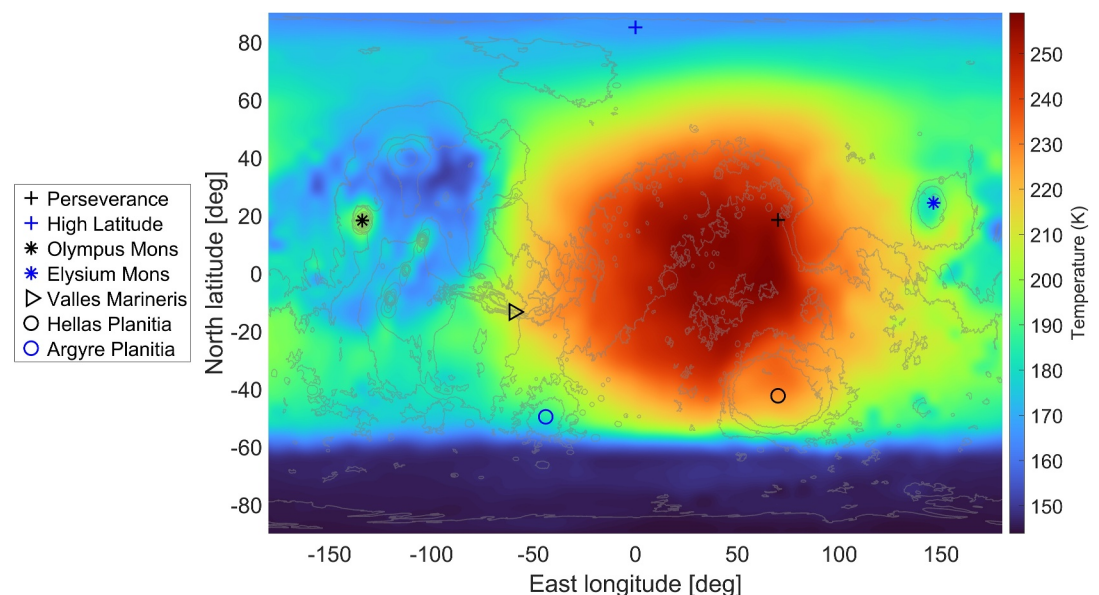


**Figure 8.** The air temperature at 3 m above the ground on Mars at  $L_s = 180^\circ$  and 12 Universal Martian Solar Time. Gray lines are contour levels extracted from MOLA (Lemoine et al., 2001).

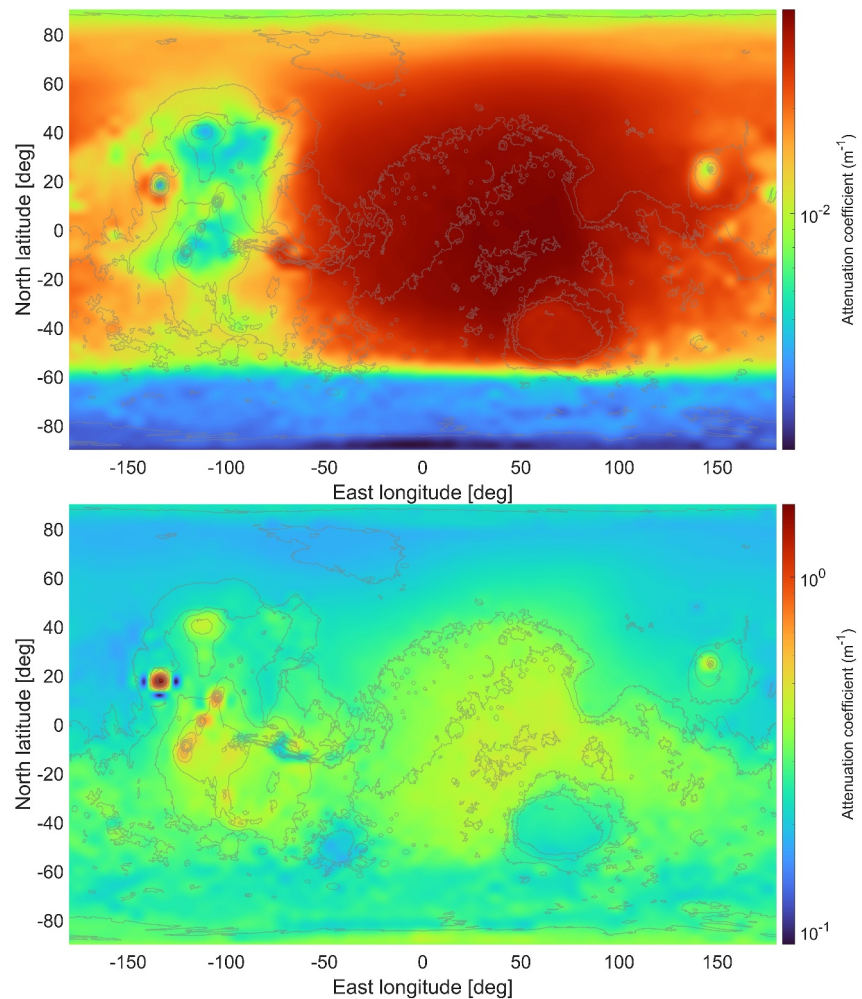


**Figure 9.** The attenuation coefficient at 100 Hz (top) and 10 kHz (bottom) at 3 m above the ground on Mars at  $L_s = 180^\circ$  and 12 Universal Martian Solar Time. Gray lines are contour levels extracted from MOLA data (Lemoine et al., 2001).

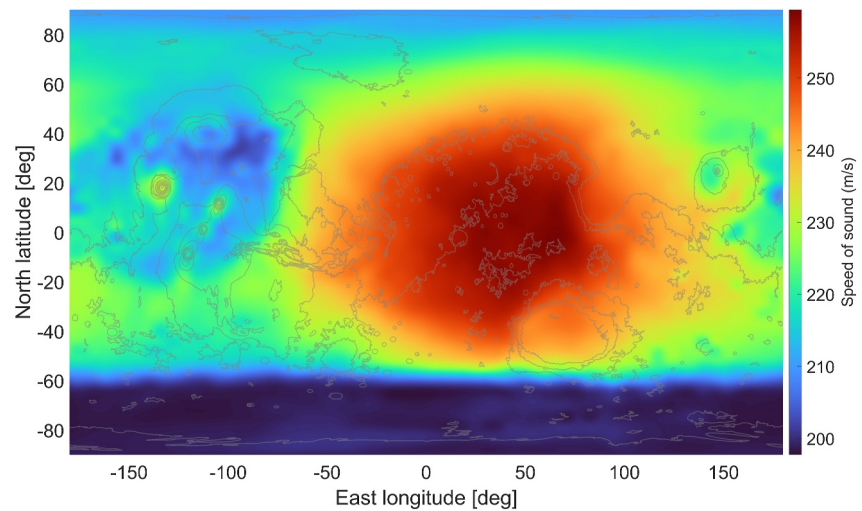
### 3.4.1. Attenuation Coefficient

Figure 9 shows the distributions of the attenuation coefficient at 100 Hz and 10 kHz across the Martian surface. The attenuation coefficient at 100 Hz follows the variation of temperature shown in Figure 8, which was expected given its sensitivity to temperature that was discussed in Section 3.3.1.

One could be surprised that the attenuation at the top of Olympus Mons and Elysium Mons is stronger than at their base. Indeed, the high altitude of these volcanoes (21 and 14 km) mean that the air density at their top is several times (2–15) smaller than at their base and, given Equations 2 and 3, one would expect that the attenuation will also be several times smaller. However, at 100 Hz the non-classical attenuation dominates over the classical one (see Figure 2). Thus there is a higher attenuation coefficient at 100 Hz as there is a slightly higher nighttime temperature at the top of these volcanoes.

On the contrary at 10 kHz, where the classical attenuation dominates, the effect of the density is important enough that the attenuation coefficient is high at the top of the volcanoes and small in the lower area of Argyre Planitia, Hellas Planitia, and Valles Marineris.





**Figure 10.** The speed of sound at 100 Hz at 3 m above the ground on Mars at  $L_s = 180^\circ$  and 12 Universal Martian Solar Time. Gray lines are contour levels extracted from Mars Orbiter Laser Altimeter (Lemoine et al., 2001).

### 3.4.2. Speed of Sound

Figure 10 shows the distributions of the speed of sound at 100 Hz across the Martian surface. As expected from Section 3.3.2, the variation of the speed of sound closely follows the variation of temperature. This is also true for the speed of sound at high frequency (10 kHz).

Global maps of the Martian surface provide a good way of showing the ranges of the attenuation coefficient and the speed of sound in one glance, but to investigate in more detail every parameter that has an impact on acoustic propagation we need to focus on a few locations. In the next section, we will focus on the Perseverance site and the high latitude site that were both marked on Figure 8.

### 3.5. Effect of the Season

In this section, the variation of the attenuation coefficient and the speed of sound along the Martian year are discussed. As the seasonal variation of the atmosphere depend on latitude, they are computed at two locations: at the Perseverance site ( $18.45^\circ\text{N}$ ,  $77.4^\circ\text{E}$ ) and at a high latitude ( $85^\circ\text{N}$ ,  $0^\circ\text{E}$ ). All values are for an altitude of 3 m and a local time of 12 LTST.

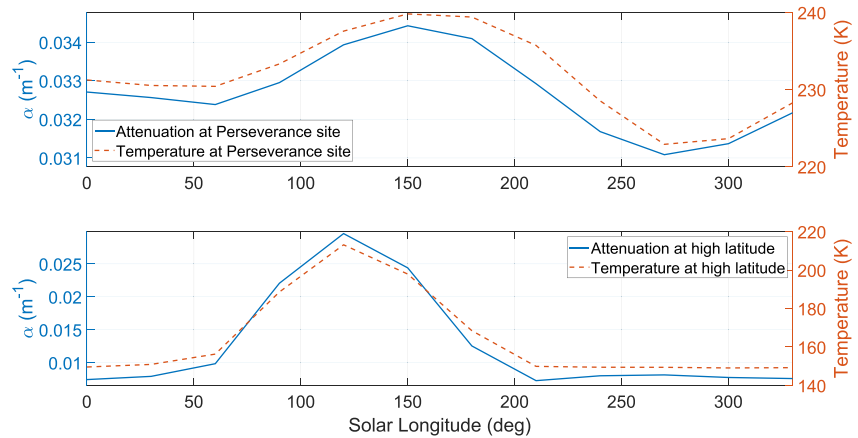
#### 3.5.1. Attenuation Coefficient

Figure 11 presents the variation of the attenuation coefficient at 100 Hz with the solar longitude. The variation in temperature is also shown. As expected from Figure 4, the variation of attenuation is predominantly explained by the variation in temperature. The variation near the Perseverance site is small, the minimum attenuation coefficient ( $L_s = 270^\circ$ ) is only 10% smaller than the maximal attenuation coefficient ( $L_s = 150^\circ$ ). On the contrary, the variation at the high-latitude site is extreme, with a minimum attenuation coefficient ( $L_s = 210^\circ$ ) 75% smaller than the maximal attenuation coefficient ( $L_s = 120^\circ$ ). This reflects the seasonal temperature cycle, which is more pronounced at high latitudes.

However, the temperature is not the only atmospheric parameter that changes along the Martian year. Because of the seasonal condensation and sublimation of  $\text{CO}_2$  at the poles, the pressure varies by 30% over the year. The volume mixing ratio of  $\text{CO}_2$  is also affected by the  $\text{CO}_2$  annual cycle: it dives to 75% at a latitude of  $85^\circ\text{N}$  near the northern winter solstice ( $L_s = 270^\circ$ ).

Figure 12 presents the effects of the variation of the pressure and the  $\text{CO}_2$  molar fraction on attenuation. These effects were estimated by simulating atmospheres with either a constant pressure or a constant chemical composition over the Martian year and comparing the results with the complete simulation presented in Figure 11. They are expressed as percentages.





**Figure 11.** Variation of the attenuation coefficient at 100 Hz with the solar longitude. The variation in temperature is also shown. The values were extracted from the Martian Climate Database at two locations: at the Perseverance site (18.45°N, 77.4°E) and at a high latitude site (85°N, 0°E). All values are for an altitude of 3 m and a local time of 12 Local True Solar Time.

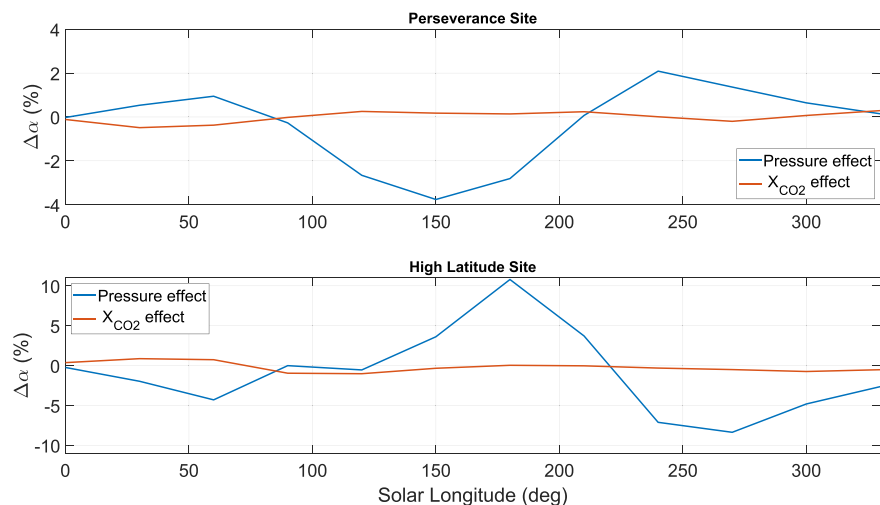
Figure 12 shows that the effect of the seasonal changes in CO<sub>2</sub> molar fraction at the Perseverance site is very small, less than 0.5%. For pressure the effect is larger but still less than 4%. At the high latitude site, the effect can go as high as an 11% increase of the attenuation coefficient because of the changes in pressure, which is more notable. For example, an 11% increase in the attenuation coefficient means that the maximum distance at which a sound source can be detected decreases by 9%.

To summarize, the change of season affects the speed of sound mainly through the associated change in temperature, which is higher at high latitude, and to a second order through the change in the pressure and the atmosphere chemical composition.

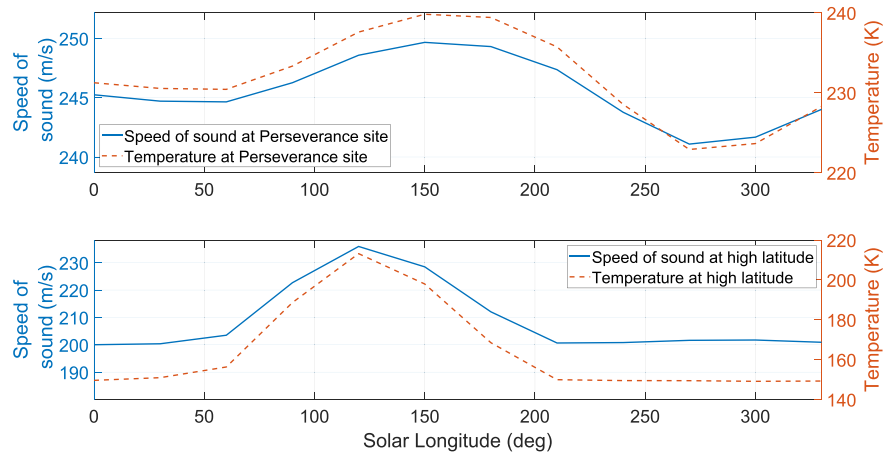
### 3.5.2. Speed of Sound

Figure 13 presents the variation of the speed of sound at 100 Hz with the solar longitude.

The variation in temperature is also shown. As expected from Figure 5, the variation of speed of sound is predominantly explained by the variation in temperature. The speed of sound is lower and more variable at high



**Figure 12.** The effects of the variation of the pressure and the CO<sub>2</sub> molar fraction on attenuation at 100 Hz, expressed as percentages of change from the mean value over the year. The atmospheric parameters were extracted from the Martian Climate Database at two location: at the Perseverance site (18.45°N, 77.4°E) and at a high latitude (85°N, 0°E). All values are for an altitude of 3 m and a local time of 12 Local True Solar Time.



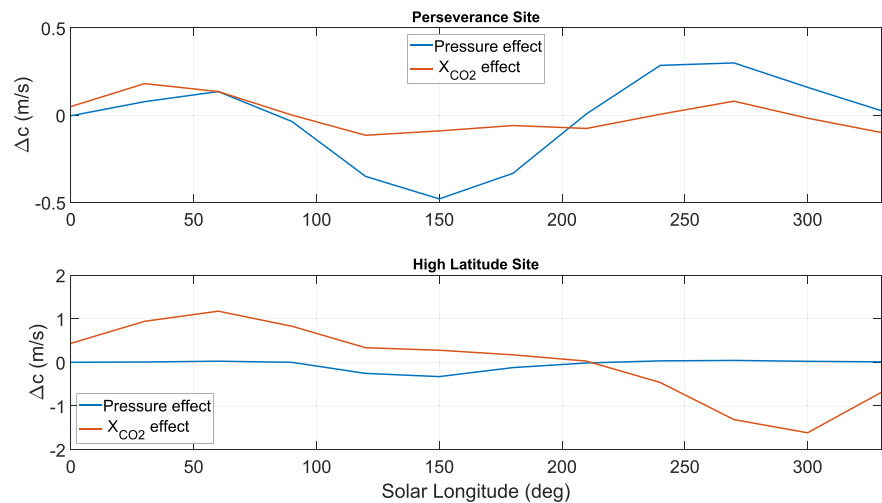
**Figure 13.** Variation of the speed of sound at 100 Hz with the solar longitude. The variation in temperature is also shown. The values were extracted from the Martian Climate Database at two locations: at the Perseverance site (18.45°N, 77.4°E) and at a high latitude (85°N, 0°E). All values are for an altitude of 3 m and a local time of 12 Local True Solar Time.

latitude, compared to the Perseverance site, because of the lower temperature and the wider temperature variations.

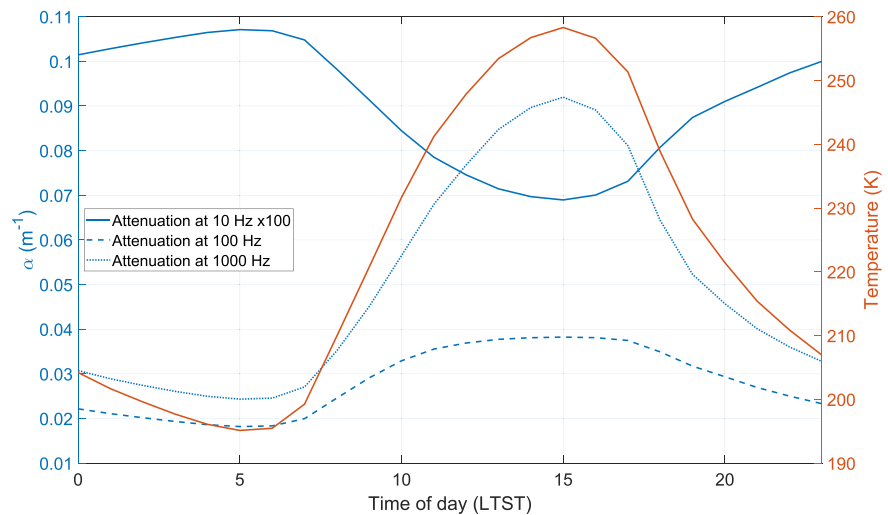
As for the attenuation coefficient, it is worth looking at the effect of the changes of the others atmospheric parameters. Figure 14 presents the effects of the variation of the pressure and the CO<sub>2</sub> molar fraction on the speed of sound. These effects were estimated by simulating atmospheres with a constant pressure (respectively chemical composition) over the Martian year and comparing the results with the complete simulation presented in Figure 13. They are expressed as speed differences in m/s.

Figure 12 shows that the effect of the seasonal changes in pressure and CO<sub>2</sub> molar fraction at the Perseverance site is smaller than at high latitudes. At high latitudes, it is the effect of the changes in CO<sub>2</sub> molar fraction that dominates, with a deviation from the mean that can go up to 1.8 m/s.

To summarize, the change of season affects the speed of sound mainly through the associated change in temperature, which is higher at high latitude, and to a second order through the change in the atmosphere chemical composition.



**Figure 14.** The effects of the variation of the pressure and the CO<sub>2</sub> molar fraction on the speed of sound at 100 Hz, expressed as a difference from the mean value over the year in m/s. The atmospheric parameters were extracted from the Martian Climate Database at two location: at the Perseverance site (18.45°N, 77.4°E) and at a high latitude (85°N, 0°E). All values are for an altitude of 3 m and a local time of 12 Local True Solar Time.



**Figure 15.** The attenuation coefficient at 10,100, and 1,000 Hz during a typical Martian day. The data necessary to compute the coefficients, including the air temperature, were extracted from the Martian Climate Database at the Perseverance site at a height of 3 m and  $L_s = 180^\circ$ .

In the following sections, we will focus on the Perseverance site at a solar longitude of  $180^\circ$ .

### 3.6. Effect of the Diurnal Cycle

An important characteristic of the Martian near-surface that is relevant for the acoustic is the diurnal temperature cycle. This cycle is well-known thanks to the numerous meteorological packages that operated on the surface of Mars (Davy et al., 2010; Gómez-Elvira et al., 2013; Munguira et al., 2023; Schofield et al., 1997; Sutton et al., 1978). The temperature is minimal around sunrise (6 LTST) and maximal in the beginning of the afternoon (15 LTST) with a range in the order of 50 K. As expected from the results of Section 3.3 these large differences have a strong impact on the attenuation coefficient and the speed of sound. Measurements of the diurnal cycle of pressure in Jezero (Sánchez-Lavega et al., 2023) have shown that its range, less than 30 Pa, is too small to affect significantly the attenuation. The range of the  $\text{CO}_2$  molar fraction over a day extracted from the MCD is 1 part per 10,000 and is thus too small to affect the attenuation or the speed of sound.

#### 3.6.1. Attenuation Coefficient

Figure 15 presents the attenuation coefficient at 10, 100, and 1,000 Hz during a typical Martian day along with the air temperature. These three frequencies were chosen to illustrate the different effects of the temperature on the attenuation coefficient.

As expected from Figure 4 the variations of attenuation at 100 and 1,000 Hz follow closely the variation of the air temperature whereas the attenuation coefficient at 10 Hz varies in the opposite direction. The considerable range in temperature (62 K) translates into an important variation of the attenuation coefficients. Hence, the maximum attenuation at 1,000 Hz is three times the minimum, whereas the attenuation coefficient at 100 Hz goes from 0.018 to 0.038  $\text{m}^{-1}$  (a factor of  $\sim 2$ ) from 5 to 15 LTST. This means that a 100 Hz sound heard at a distance of 100 m will have a sound intensity 17 dB smaller at 15 LTST than at 5 LTST or equivalently that the maximum distance at which a specific sound can be heard will be two times smaller at 15 LTST than at 5 LTST (neglecting geometric spreading).

To summarize, throughout the day, the strong variation in air temperature near the Martian surface is the leading factor causing the strong variation of the attenuation coefficient.

#### 3.6.2. Speed of Sound

Figure 16 presents the speed of sound at 10, 100, and 1,000 Hz during a typical Martian day along with the air temperature.

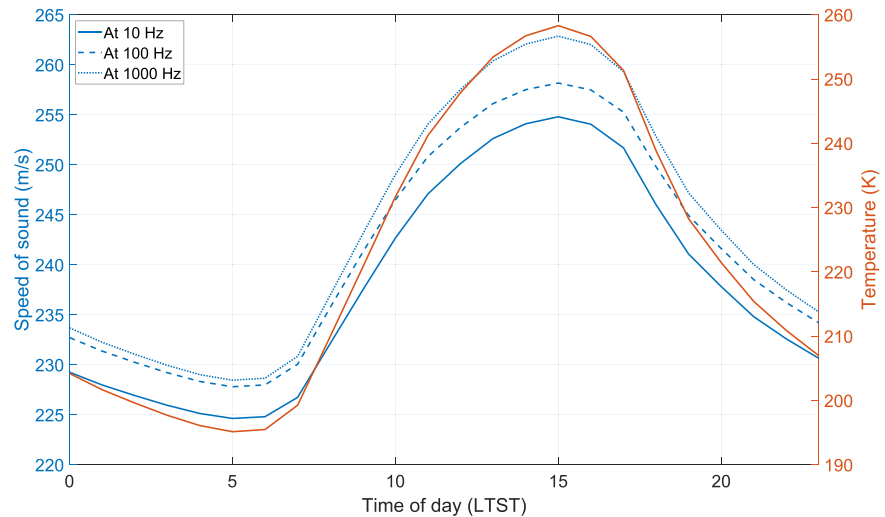


**Figure 16.** The speed of sound at 10, 100, and 1,000 Hz during a typical Martian day. The data necessary for the computation of the coefficients, including the air temperature, were extracted from the Martian Climate Database at the Perseverance site at a height of 3 m and  $L_s = 180^\circ$ .

Figure 13 shows that the considerable differences in temperature that occur along a Martian day are responsible for a variation of speed of sound of 30 m/s for frequencies of 10 and 100 Hz and 40 m/s for a frequency of 1 kHz. This corresponds to an increase of  $\sim 15\%$ . For comparison, if the temperature goes from 0 to  $20^\circ\text{C}$  during a typical day on Earth, the corresponding increase of temperature will be only around 3%. Compared to the result of Section 3.5, this also means that the speed of sound variations throughout a diurnal cycles at 100 Hz are three times higher than the variations during a seasonal cycle.

To summarize, across the day, the strong variation in air temperature near the Martian surface is causing strong variations of the speed of sound.

### 3.7. Near-Surface Profiles

Profiles of attenuation and speed of sound going from the Martian surface to the top of the atmosphere have already been presented in Petculescu and Lueptow (2007). Here we will focus on the first 20 m of the Martian atmosphere as it is the place where landers, rovers and drones operate. In-situ measurements of the Martian temperature profile (Munguira et al., 2023; Smith et al., 2006) have shown that they present a consistent diurnal pattern, with a stable stratified atmosphere during the night and a strong super-adiabatic vertical gradient from mid-morning to mid-afternoon. As a consequence, temperature profiles are shown for different local times. The pressure gradient is very small, with less than 2 Pa of difference between the ground and 20 m of altitude. The chemical composition does not vary over such a short distance.

Figure 17 shows temperature profiles over the first 20 m of the Martian atmosphere at different times of day.

At midnight, the atmosphere is stably stratified with a positive temperature gradient. Then soon after sunrise, that occurs at 6 LTST, the temperature profile reverses to a negative temperature gradient. At midday, the range of temperature between the ground and 20 m high is the strongest of the day (47 K). Then, just before the sunset that occurs at 18 LTST, the temperature profile reverses again.

#### 3.7.1. Attenuation Coefficient

Figure 18 shows the attenuation coefficient profiles at 100 Hz and 1 kHz over the first 20 m of the Martian atmosphere at different times of day.

The variations of the attenuation coefficient with altitude closely follow the variations of temperature. The difference between the attenuation coefficient at the ground level and at 2 m can reach 90% at 1 kHz, but reduces to less than 10% at 100 Hz. This means that, at midday, a sound wave in the kilohertz range going through the 2 first meters of the atmosphere will be considerably more attenuated than the same sound wave traveling a few meters

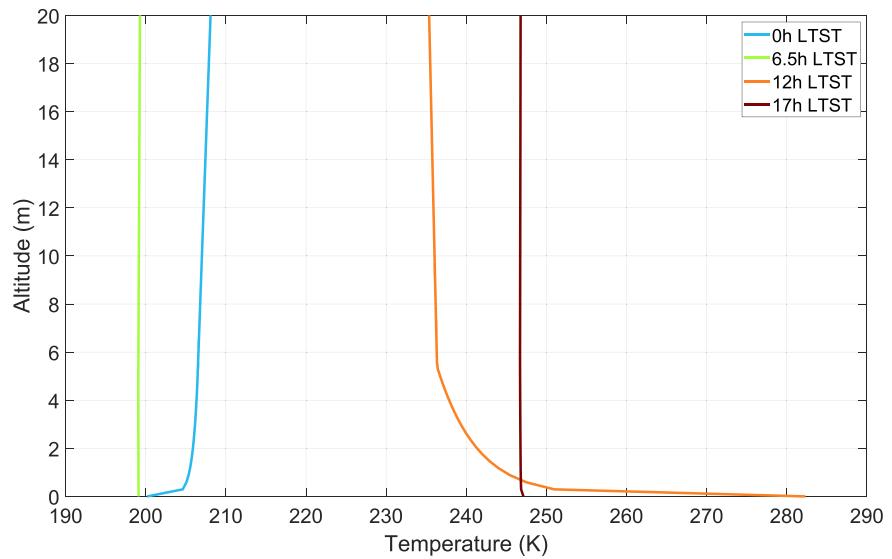


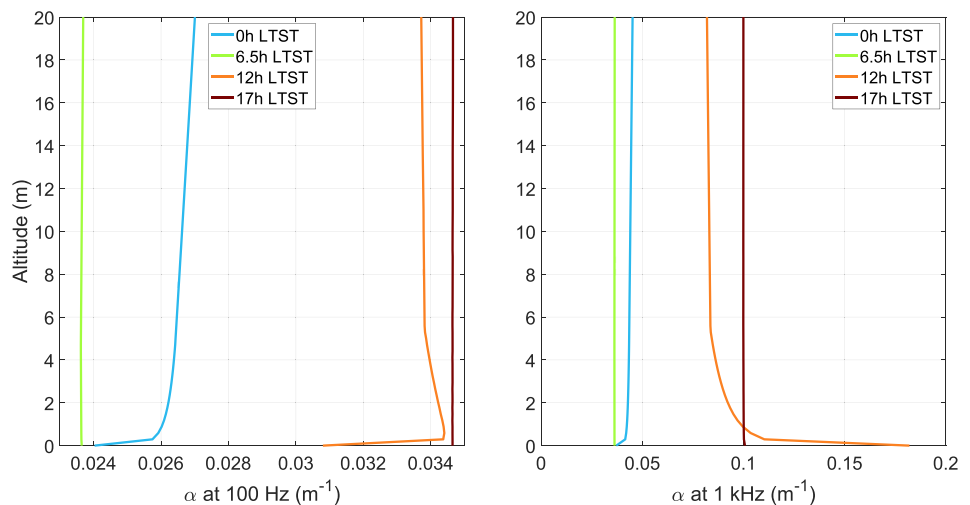
**Figure 17.** The temperature profiles over the first 20 m of the Martian atmosphere at different times of day. Data extracted from the Martian Climate Database at the Perseverance site at  $L_s = 180^\circ$ .

above. Hence, when designing acoustic instruments intended to operate in this layer, it is crucial to take these variations of temperature and thus attenuation into account.

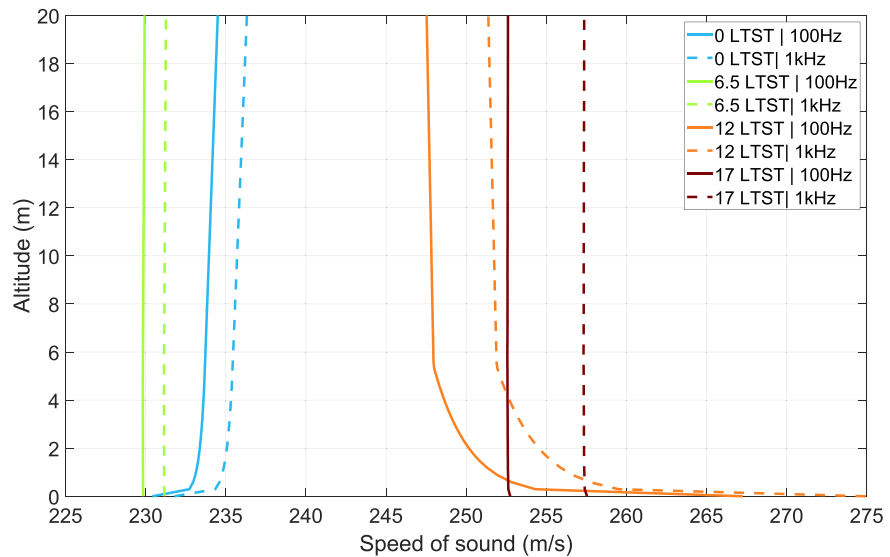
### 3.7.2. Speed of Sound Coefficient

Figure 19 presents the speed of sound profiles at 100 Hz and 1 kHz over the first 20 m of the Martian atmosphere at different times of day.

Again, the variations in speed of sound follow the variation in temperature. The difference of speed of sound between the ground and 2 m high at midday is around 17 m/s which is considerably higher than the value of 3 m/s that is given for a typical speed of sound profile over similar distances on Earth in Salomons (2001). This strong gradient is negative, which means that sound waves traveling through the first 2 m are bent upward.



**Figure 18.** The attenuation coefficient profiles at 100 Hz and 1 kHz over the first 20 m of the Martian atmosphere at different times of day. Data extracted from the Martian Climate Database at the Perseverance site at  $L_s = 180^\circ$ .



**Figure 19.** The speed of sound profiles at 100 Hz and 1 kHz over the first 20 m of the Martian atmosphere at different times of day. Data extracted from the Martian Climate Database at the Perseverance site at  $L_s = 180^\circ$ .

## 4. Discussion

### 4.1. The Variation of the Acoustic Impedance of the Air

In Section 3 we only considered the propagation losses that occur when the sound wave is traveling in the atmosphere. However, losses can also occur at the interface between the sound source and the atmosphere, and between the atmosphere and the microphone. This is characterized by the acoustic impedance of the air,  $Z_{air} = \rho c$  where  $\rho$  is the atmospheric density and  $c$  the speed of sound. Compared to Earth, the lower air density at the Martian surface ( $0.02 \text{ kg/m}^3$  compared to  $1.2 \text{ kg/m}^3$ ) and the lower speed of sound ( $240 \text{ m/s}$  compared to  $340 \text{ m/s}$ ) mean that the acoustic impedance of air at the Martian surface is almost 100 times smaller than on Earth ( $4.8 \text{ kg/m}^2\text{s}$  compared to  $408 \text{ kg/m}^2\text{s}$ , see Petculescu and Lueptow (2007) for comparison with other planetary bodies and other types of material). This means that acoustic waves emitted into the atmosphere by a source of equal surface velocity magnitude will be 40 dB weaker on Mars than they would be on Earth.

Moreover, it is important to note that the large changes in pressure across the Martian year (see Section 3.5) cause strong variations in the acoustic impedance of air. This means that, even if the changes of pressure only have a small impact on the attenuation of the sound waves, they have a strong impact on the coupling between the sound source and the atmosphere, and the atmosphere and the microphone. Thus, the signal on the microphone would vary regardless of propagation losses. This has already been observed on Mars (Chide et al., 2023).

### 4.2. Limits of the Physics-Based Acoustic Model

One limit of the acoustic model at high frequency is the continuum medium hypothesis. Indeed, if the acoustic Knudsen number, that is, the ratio between the mean free path and the wavelength, is too big (e.g., greater than 0.01) the gas can no longer be considered continuous and other equations should be used. This is especially important in the thin Martian atmosphere, where the mean free path can be as large as  $50 \mu\text{m}$  near the surface (and larger at higher altitudes). This means that Knudsen number is greater than 0.01 for frequency greater than 50 kHz. This is important for the study of ultrasonic sources, such as potential future ultrasonic anemometers. This will also be important when considering the ground-air interaction to predict the ground impedance and model sound propagation in the presence of the ground.

In the previous sections, all the calculations were made assuming that the Martian atmosphere does not contain water vapor (see Table 1). However, models (H. Bass et al., 1984) and experiments (Zuckerwar & Meredith, 1985) have shown that the sound attenuation coefficient in Earth's atmosphere is highly dependent on the amount of water vapor in air. The Martian atmosphere is very dry compared to Earth's (Montmessin et al., 2017). In-situ measurements at Perseverance site (Polkko et al., 2023) have shown that the maximum nighttime volume



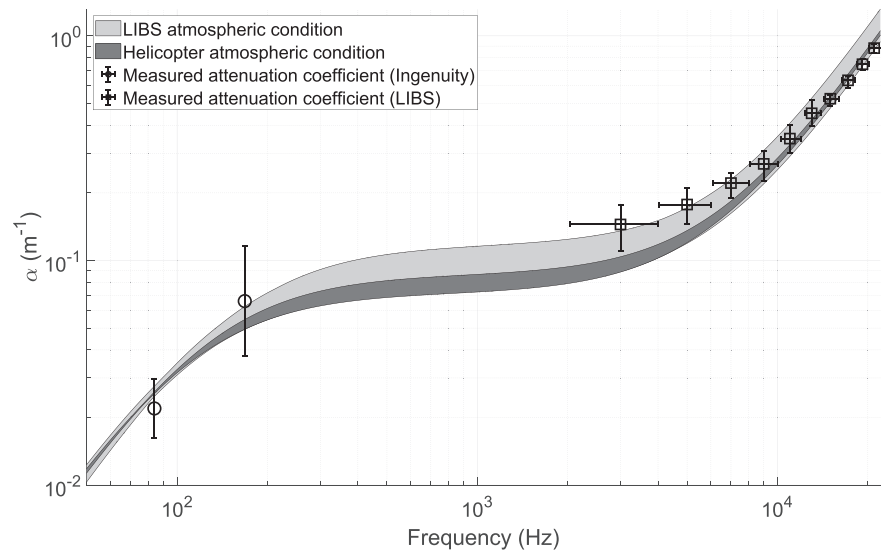


**Figure 20.** The measured attenuation coefficient (Chide et al., 2023) compared to the outputs of the physics-based acoustic model. The light gray area is the predicted range of attenuation coefficient for the laser-induced breakdown spectroscopy atmospheric conditions ( $L_s = 0^\circ\text{--}360^\circ$ , Local True Solar Time (LTST) from 11 to 14 and an altitude of 0.9 m), the dark gray area is the predicted range of attenuation coefficient for the helicopter atmospheric condition ( $L_s = 38^\circ\text{--}48^\circ$ , LTST from 11 to 13 and an altitude of 6 m).

mixing ratio of water vapor depends on the season and is always under 120 ppm. During daytime, the relative humidity is too low to derive a volume mixing ratio, but models (Polkko et al. (2023), and MCD) show that it stays under 500 ppm. The attenuation coefficient computed by the PBAM for a Martian atmosphere with 500 ppm water do not differ by more than 1% from that of the dry atmosphere. However, experimental work points to the vibrational relaxation of  $\text{CO}_2$  by  $\text{H}_2\text{O}$  being unusually rapid. Different explanations have been proposed to explain this fast rate of energy exchange, such as a chemical affinity between the two molecules (Widom & Bauer, 1953) or rapid near resonant transfer of vibrational energy of  $\text{CO}_2$  to rotational energy of  $\text{H}_2\text{O}$  (Sharma, 1971). This means that, in the current implementation, the PBAM underestimates the effect of water vapor on the attenuation coefficient of the Martian atmosphere. By comparison, the attenuation coefficient predicted by H. E. Bass and Chambers (2001) leads to a non-negligible effect of water vapor at Martian surface conditions.

Future models could account for water vapor effects by using interaction potentials appropriate for the polar nature of water molecules to correctly simulate the relaxation of  $\text{CO}_2$  by  $\text{H}_2\text{O}$ .

### 4.3. In Situ Experimental Validation

The presence of an operational microphone at the surface of Mars (Mimoun et al., 2023) that motivated in part this work also allows the comparison of the outputs of the model to in-situ experimental data. Measurements of speed of sound (Maurice et al., 2022) and attenuation coefficient (Chide et al., 2023) have been published at different frequencies using the helicopter and the LIBS instrument. The helicopter produces sound at its blade passage frequency, 84 Hz, and its first harmonic 168 Hz (R. D. Lorenz et al., 2023) whereas LIBS sounds ranges from 3 to 21 kHz (Chide et al., 2023). The helicopter flies at an altitude of 5–10 m above the ground, the microphone is 1.8 m from the ground and the LIBS experiment shockwaves are located on the ground.

Figures 20 and 21 show the measured attenuation and speed of sound compared to the outputs of the PBAM model for two situations, corresponding to the experimental conditions when measuring with the helicopter and the LIBS. The helicopter atmospheric conditions are the outputs of the MCD for  $L_s$  between  $38^\circ$  and  $48^\circ$ , LTST between 11 and 13 and an altitude of 6 m. The LIBS atmospheric conditions are the outputs of the MCD for  $L_s$  between  $0^\circ$  and  $360^\circ$ , LTST between 11 and 14 and an altitude of 0.9 m.

Figure 20 shows that every attenuation coefficient data point falls within the predicted value range once the error bars are taken into account. The error bars are very large, especially for the helicopter, when compared to the

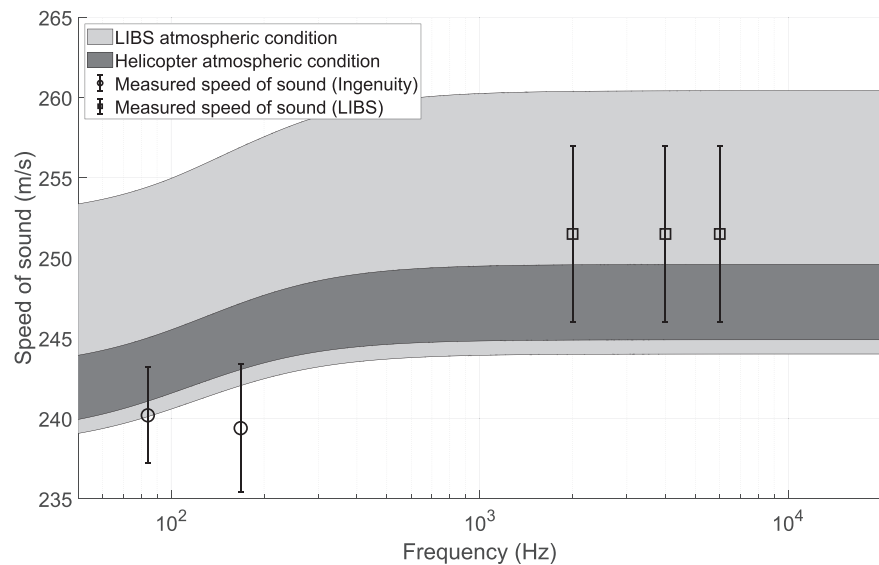


**Figure 21.** The measured speed of sound (Maurice et al., 2022) compared to the outputs of the physics-based acoustic model. The light gray area is the range of speed of sound for the laser-induced breakdown spectroscopy atmospheric conditions ( $L_s = 0^\circ\text{--}360^\circ$ , Local True Solar Time (LTST) from 11 to 14 and altitude = 0.9 m), the dark gray area is the range of speed of sound for the helicopter atmospheric condition ( $L_s = 38^\circ\text{--}48^\circ$ , LTST from 11 to 13 and altitude = 6 m). For the helicopter, the wind speed at the time of flight was taken into account.

differences between the different attenuation models (see Figure 3) or even the difference that a 10 K increase in air temperature makes to attenuation (see Figure 4) and thus these measurements can not be used to discriminate between the different models or to validate the temperature dependency of the attenuation coefficient.

Figure 21 shows that every sound speed data point falls within the predicted value range once the error bars are taken into account. However, the predicted range of speed of sound for the LIBS conditions is very large, given its sensitivity to air temperature and the wide variations of air temperature near the ground over the year. The variations of the LIBS-derived speed of sound with temperature has been studied in Chide et al. (2022). For the helicopter, the predicted speeds seem to be high compared to the measured ones. This could be explained by the fact that during the time of flight, wind was blowing from the microphone to the helicopter. This wind velocity that was taken into account was measured at the rover wind sensor height (1.5 m), whereas the true wind speed between the rover and the helicopter may have been larger at an altitude of 5–10 m.

In any case, in these two in-situ experiments, sound waves are not traveling parallel to the ground and are thus traversing layers of atmosphere that can have very different properties, as shown in Section 3.7.

To summarize, while the in-situ experimental results are generally in line with the model predictions, we need to look more closely at the sensitivity of the measured attenuation and speed of sound to atmospheric parameters and understand the sound propagation paths in the Martian atmosphere, in order to conclude on the validity of the model.

#### 4.4. Perspective and Future Work

This work presents a method to compute the sound attenuation and speed at any point of the Martian surface at any time and date. At a first order, one could estimate the acoustic losses between a sound source and a detector by applying this attenuation coefficient to the distance between the source and the detector. However, sound waves are usually not traveling straightforwardly in the atmosphere. Indeed, the fact that speed of sound changes with altitudes (see Section 3.7) means that sound waves are refracted. Moreover, to compute the effective speed of sound, the wind profile must be taken into account. Finally, the turbulent fluctuations of the atmosphere, that are particularly strong close to the ground, can also impact the way sound propagates near the surface. Hence, to model accurately the sound field created by a particular sound source, a model of atmospheric sound propagation is needed. This will be the subject of future work.

## 5. Conclusion

The model presented in this work can be used to compute the acoustic attenuation coefficient and the speed of sound near the Martian surface at any location, any time of year and any time of day for a wide range of frequencies. It has shown that the presence of airborne dust has a negligible impact on sound attenuation and speed. Attenuation of sound waves under 8 kHz is dominated by the non-classical attenuation which is sensitive to temperature, whereas attenuation above 8 kHz is dominated by classical attenuation which is sensitive to both pressure and temperature through air density. Consequently the large diurnal cycle of temperature at the Martian surface is responsible for a variation in the value of the attenuation coefficient that can be as much as three times greater during the hottest hours than during the coldest ones. The speed of sound in turn is sensitive mainly to temperature and at a second order to the atmosphere chemical composition. As a result, the variation of speed of sound across the Martian year is primarily caused by the diurnal cycle of temperature and by seasonal changes in temperature and chemical CO<sub>2</sub> molar fraction, which are stronger at high latitudes. The diurnal cycle of air temperature profile in the first 20 m of the Martian creates important differences between the speed of sound profiles at night and during the day: at midday, the speed of sound gradient in the first 2 m of the atmosphere is very strong compared to Earth.

## Acronyms

<b>CNSA</b>	Chinese National Space Administration
<b>EDL</b>	Entry Descent and Landing
<b>LIBS</b>	Laser-Induced Breakdown Spectroscopy
<b>LTST</b>	Local True Solar Time
<b>MCD</b>	Martian Climate Database
<b>MOLA</b>	Mars Orbiter Laser Altimeter
<b>NASA</b>	National Aeronautics and Space Administration
<b>PBAM</b>	Physics-Based Acoustic model
<b>UMST</b>	Universal Martian Solar Time

## Notation

$a$	Particle radius in a suspension
$A_0$	Calibration constant corresponding to the pressure received at a reference distance
$c$	Speed of sound
$c_{Tf}$	Isothermal speed of sound of the fluid in a suspension
$c_p$	Specific heat at constant pressure
$k$	Wavenumber (can be complex)
$K$	Thermal conductivity
$k_{dust}$	Wavenumber in the presence of dust (complex)
$k_{eff}$	Effective wavenumber in the presence of molecular vibrations (complex)
$k_0$	Real part of the wavenumber
$L_s$	Solar longitude
$M$	Molar mass
$r$	Distance to the sound source
$\alpha$	Attenuation coefficient

$\alpha_{class}$	Classical attenuation coefficient
$\alpha_{non-class}$	Non-classical attenuation coefficient
$\alpha_{nu}$	Attenuation coefficient associated with viscous losses
$\alpha_{vib}$	Attenuation coefficient associated with molecular vibrations
$\alpha_t$	Attenuation coefficient associated with heat transfers
$\delta$	Fluid to particle density ratio in a suspension
$\eta$	Coefficient of shear viscosity
$\gamma$	Heat capacity ratio
$\nu_f$	Kinematic viscosity of the fluid in a suspension
$\nu_i$	Wavenumber of vibration mode number $i$ ( $i = 1, 2, 3$ ) of CO <sub>2</sub>
$\omega$	Angular frequency
$\phi_v$	Volume concentration of particle in a suspension
$\rho$	Density of the gas mixture
$\tau_d$	Dynamical relaxation time for a particle in a suspension

### Appendix A: Acoustic Model Description

This appendix describes step by step the implementation of the acoustic model used in this work. It is based on the work presented in Dain and Lueptow (2001), Petculescu and Lueptow (2005).

Let us consider a gas mixture of made of  $M$  different molecules. In some of these molecule, the atoms can be vibrating relatively to each other. These vibrations follow modes that are characterized by their vibrational frequency  $n_i$  and their vibrational wavenumber  $\nu_i$ . They are related by:

$$n_i = c_l \nu_i \quad (A1)$$

with  $c_l$  the speed of light. Let us note  $N$  the total number of modes in the gas mixture.

The acoustic equations for this gas mixture can be written as:

$$\begin{aligned} \frac{p}{\rho_0} &= \frac{T}{T_0}, \frac{\partial p}{\partial t} + \rho_0 \frac{\partial u}{\partial x} = 0, \frac{\partial u}{\partial t} + \rho_0^{-1} \frac{\partial p}{\partial x} = 0 \\ \frac{\partial \epsilon}{\partial t} - \rho_0 \rho_0^{-2} \frac{\partial p}{\partial t} &= 0 \\ \epsilon &= c_v T + \sum_{i=1}^n \alpha_i c_i^{vib} T_i^{vib} \end{aligned} \quad (A2)$$

with  $p$ ,  $\rho$ ,  $u$ ,  $\epsilon$ , and  $T$  the small fluctuations of the pressure, density, velocity, energy, and temperature around the equilibrium values that are indexed by 0. Here  $\alpha_i$  is the molar fraction of the molecule that correspond to mode number  $i$ ,  $c_i^{vib}$  is the vibrational specific heat capacity of mode  $i$  and  $T_i^{vib}$  is the associated internal temperature.  $c_v$  is the isochoric specific heat capacity,  $t$  is time and  $x$  is the spatial coordinate.

The goal of the model is to compute the effective wavenumber,  $k_{eff}$  which is the wavenumber that take into account the internal degree of freedom of the molecules. The expression of  $k_{eff}$  by analogy with the regular wavenumber, is:

$$k_{eff}(f) = 2\pi f \sqrt{\frac{\rho_0 c_v^{eff}(f)}{p_0 c_p^{eff}(f)}}, \quad (A3)$$

where  $c_v^{eff}$ , and  $c_p^{eff}$  are the effective isochoric and isobaric specific heat capacities. These complex numbers represent the specific heat capacities of the gas mixture in the presence of molecular vibrations. By definition, the effective specific isochoric heat capacity is such that  $\epsilon \equiv c_v^{eff} T$  and thus by identification with Equation A2:

$$c_v^{eff} \equiv c_v + \sum_{i=1}^N x_i c_i^{vib} \frac{T_i^{vib}}{T} \equiv c_v + \sum_{i=1}^N x_i c_i^{vib} \Gamma_i \quad (A4)$$

with  $\Gamma_i = \frac{T_i^{vib}}{T}$  the temperature ratio.

To compute the vibrational specific heat, the Planck-Einstein function for a harmonic oscillator is used:

$$c_i^{vib} = g_i R \left( \frac{\theta_i^{vib}}{T_0} \right) \frac{\exp(\theta_i^{vib}/T_0)}{(\exp(\theta_i^{vib}/T_0) - 1)^2}, \theta_i^{vib} = \frac{hn_i}{k_B} \quad (A5)$$

where  $h$  is Planck's constant,  $R$  is the ideal gas constant,  $k_B$  is Boltzmann's constant and  $g_i$  is the degeneracy of the mode  $i$ .

To compute the temperature ratios, one must use the relaxations equations of the internal temperatures that were established by Landau (1936), Schwartz et al. (1952):

$$\frac{dT_i^{vib}}{dt} \approx \frac{T - T_i^{vib}}{\tau_i^{V-T}} + \sum_{k \neq i} \frac{1}{\tau_{i,k}^{V-V}} \frac{1 - \exp(-hn_i/k_B T_0)}{1 - \exp(-hn_k/k_B T_0)} \times \left[ (T - T_i^{vib}) - \frac{n_k}{n_i} (T - T_k^{vib}) \right] \quad (A6)$$

where  $\tau_i^{V-T}$  is the translational relaxation time, that is, the time for a molecule that was vibrating in mode  $i$  to lose energy to molecular translation in a collision, and  $\tau_{i,k}^{V-V}$  is the paired vibrational relaxation time, that is, the time for a molecule that was vibrating in mode  $i$  to lose energy to molecular vibration in mode  $k$  in a collision.

The expression of the translational relaxation times is:

$$(\tau_i^{V-T})^{-1} = \sum_{j=1}^M \frac{\alpha_j}{\tau_{i,j}^{V-T}} \quad (A7)$$

$$(\tau_{i,j}^{V-T})^{-1} = Z(i,j) P_{0 \rightarrow 0}^{1 \rightarrow 0}(i,j) (1 - \exp(-hn_i/k_B T_0)) \quad (A8)$$

And the expression of the paired vibrational relaxation times is:

$$(\tau_{i,k}^{V-V})^{-1} = \alpha_k g_k Z(i,k) P_{0 \rightarrow 1}^{1 \rightarrow 0}(i,k) \quad (A9)$$

Here  $Z(i, k)$  is the collision rate between the molecules with mode  $i$  and  $k$ . Modeling the molecules as hard sphere with a collision diameter  $\sigma$ , the kinetic theory gives (Lambert, 1977):

$$Z(i,k) = 2N_k \left( \frac{\sigma_i + \sigma_k}{2} \right)^2 \left( 2\pi k_B T_0 \frac{m_i + m_k}{m_i m_k} \right)^{1/2} \quad (A10)$$

where  $N_k$  is the number of molecules of species  $k$  per unit volume and  $m_i$  is the mass of molecule  $i$ .

$P_{0 \rightarrow 0}^{1 \rightarrow 0}(i, j)$  and  $P_{0 \rightarrow 1}^{1 \rightarrow 0}(i, k)$  are transitional probabilities, that is, the probability that during a collision, vibrational energy is lost to translational energy or another vibration mode. Here,  $1 \rightarrow 0$  denotes that the considered vibrational mode goes from excited to de-excited.

The expression of these probabilities is given in Tanczos (1956):

$$P_{i_b \rightarrow f_b}^{i_a \rightarrow f_a}(a, b) = P_0(a)P_0(b) \frac{1.364}{1 + C/T_0} \left( \frac{r_c}{\sigma_{ab}} \right)^2 \bar{V}_{i_a, f_a}^2 \bar{V}_{i_b, f_b}^2 \times 8\sqrt{\pi/3} \left( \frac{2\pi\mu\Delta E}{\alpha_{ab}^* \hbar^2} \right)^2 \zeta_{ab}^{1/2} \exp \left[ -3\zeta_{ab} + \frac{\Delta E}{2k_B T_0} + \frac{\epsilon_{ab}}{k_B T_0} \right] \quad (\text{A11})$$

with

$$\zeta_{ab} \equiv \frac{\mu v_0^{*2}}{2k_B T_0} = \left( \frac{\Delta E^2 \mu \pi^2}{2\alpha_{ab}^* \hbar^2 k_B T_0} \right)^{1/3} \quad (\text{A12})$$

$\Delta E = \hbar\omega_a(i_a - f_a) + \hbar\omega_b(i_b - f_b)$  is the energy exchanged with translational degrees of freedom during a collision process, with  $\omega_a = 2\pi n_a$  the vibrational angular frequency. Here  $i$  and  $f$  denote the number of quanta of the mode at the initial and final states. In this work, we consider only single quanta transition, so they are equal to 1 or 0.  $P_0$  is a non-sphericity factor, and  $C$  is the Sutherland constant.

The vibrational factors,  $\bar{V}_{i, f}^2$  are Schwartz et al. (1952):

$$\bar{V}_{i_a, f_a}^2 = \begin{cases} 1 & \text{for } f_a = i_a \\ (i_a + 1/2 \pm 1/2)(\alpha_{aa}^*)^2 \bar{A}^2 \hbar / 2\omega_a & \text{for } f_a = i_a \pm 1 \end{cases} \quad (\text{A13})$$

In these equations,  $\epsilon_{ab}$  and  $\sigma_{ab}$  are the pairwise potential depth and the collision diameter that are the parameters of the Lennard-Jones function.  $v_0^*$  is the transition-favorable incident velocity.  $\alpha_{ab}^*$  and  $r_c$  are the parameters of the exponential function that is fitted to the Lennard-Jones function following the procedure explained in Petculescu and Lueptow (2005).  $\mu \equiv m_a m_b / (m_a + m_b)$  is the reduced mass of the molecule pair.

Assuming a harmonic time dependence Equation A6 can be written in matrix form as:

$$(i\omega \mathbf{I} + \mathbf{A})T^{vib} = \mathbf{q}T \quad (\text{A14})$$

with  $\mathbf{I}$  the identity matrix and  $\mathbf{A}$  and  $\mathbf{q}$  a matrix and a vector whose component are:

$$q_i = \frac{1}{\tau_i^{v \rightarrow T}} + \sum_{k \neq i} \frac{1}{\tau_{i,k}^{v \rightarrow v}} \frac{1 - \exp(-\hbar n_i / k_B T_0)}{1 - \exp(-\hbar n_k / k_B T_0)} \left[ 1 - \frac{n_k}{n_i} \right] \quad (\text{A15})$$

$$A_{ii} = \frac{1}{\tau_i^{v \rightarrow T}} + \sum_{k \neq i} \frac{1}{\tau_{i,k}^{v \rightarrow v}} \frac{1 - \exp(-\hbar n_i / k_B T_0)}{1 - \exp(-\hbar n_k / k_B T_0)} \quad (\text{A16})$$

$$A_{i,k} = -\frac{1}{\tau_{i,k}^{v \rightarrow v}} \frac{1 - \exp(-\hbar n_i / k_B T_0)}{1 - \exp(-\hbar n_k / k_B T_0)} \frac{n_k}{n_i} \quad (\text{A17})$$

Temperature ratio  $\Gamma$  is then obtained by resolving Equation A14:

$$\Gamma \equiv \frac{T^{vib}}{T} = (i\omega \mathbf{I} + \mathbf{A})^{-1} \mathbf{q} \quad (\text{A18})$$

Effective specific heats can then be computed using Equation A4 and thus the effective wavenumber can be derived using Equation A3.



### Notation

$\bar{V}_{i,f}^2$	Vibrational factor between initial state $i$ and final state $f$
$\alpha_{ab}^*$	Repulsion parameter
$\alpha_i$	Molar fraction of the of mode $i$
$\Delta E$	Energy exchanged with translational degrees of freedom during a collision process
$\epsilon$	Fluid internal energy
$\epsilon_{ab}$	Pairwise potential depth between molecule $a$ and $b$ in the Lennard-Jones function
$\Gamma_i$	Temperature ratio of the mode $i$
$\hbar$	Reduced Planck's constant
$\mu$	Molecule pair reduced mass
$\nu_i$	Vibrational wavenumber
$\rho$	Small vibration in density
$\rho_0$	Equilibrium density
$\sigma_{ab}$	Collision diameter between molecule $a$ and $b$ in the Lennard-Jones function
$\sigma_i$	Collision diameter of molecule $i$
$\tau_{i,k}^{V-V}$	Paired vibrational relaxation time of the mode $i$ and $k$
$\tau_i^{V-T}$	Translational relaxation time of the mode $i$
$\theta_i^{vib}$	Characteristic temperature for vibration of the mode $i$
$C$	Sutherland constant
$c_i^{vib}$	Vibrational specific heat capacity of mode $i$
$c_l$	Speed of light
$c_p^{eff}$	Effective isobaric specific heat capacity
$c_v$	Isochoric specific heat capacity
$c_v^{eff}$	Effective isochoric specific heat capacity
$g_i$	Degeneracy of the mode $i$
$k_{eff}$	Effective wavenumber in the presence of molecular vibrations (complex)
$k_B$	Boltzmann's constant
$m_a$	Mass of molecule $a$
$n_i$	Vibrational frequency of a molecule vibration mode
$N_k$	Number of molecule $k$ per unit volume
$p$	Small fluctuation of pressure
$P_{i_b \rightarrow f_b}^{i_a \rightarrow f_a}(a, b)$	Transition probability between from $i_a$ and $i_b$ to $f_a$ and $f_b$ during a collision between molecule $a$ and $b$
$p_0$	Equilibrium pressure
$P_0(a)$	Steric factor of molecule $a$
$R$	Ideal gas constant

$r_c$	Point of closest approach or classical turning point for the transition-favorable incident velocity
$T$	Small vibration in temperature
$t$	Time
$T_0$	Equilibrium temperature
$T_i^{vib}$	Internal temperature of the mode $i$
$u$	Fluid velocity
$x$	Spatial coordinate
$Z(i, j)$	Collision rate between the molecules with mode $i$ and mode $j$

## Data Availability Statement

The meteorological data are from the Martian Climate Database Forget et al. (1999), Millour et al. (2018).

The code of the model and data for Figures 4–6 are available at (Gillier & Petculescu, 2023).

## Acknowledgments

We gratefully acknowledge funding from the French space agency (CNES), from ISAE-SUPAERO, and from Région Occitanie.

## References

- Ainslie, M. A., & Leighton, T. G. (2016). Sonar equations for planetary exploration. *Journal of the Acoustical Society of America*, 140(2), 1400–1419. <https://doi.org/10.1121/1.4960786>
- Bass, H., Sutherland, L., Piercy, J., & Evans, L. (1984). Absorption of sound by the atmosphere. In *Physical acoustics: Principles and methods (A85-28596 12-71)*. Orlando (Vol. 17, pp. 145–232).
- Bass, H. E., & Chambers, J. P. (2001). Absorption of sound in the Martian atmosphere. *Journal of the Acoustical Society of America*, 109(6), 3069–3071. <https://doi.org/10.1121/1.1365424>
- Chide, B., Bertrand, T., Lorenz, R. D., Munguira, A., Hueso, R., Sánchez-Lavega, A., et al. (2022). Acoustics reveals short-term air temperature fluctuations near Mars' surface. *Geophysical Research Letters*, 49(21), e2022GL100333. <https://doi.org/10.1029/2022GL100333>
- Chide, B., Jacob, X., Petculescu, A., Lorenz, R. D., Maurice, S., Seel, F., et al. (2023). Measurements of sound propagation in Mars' lower atmosphere. *Earth and Planetary Science Letters*, 615, 118200. <https://doi.org/10.1016/j.epsl.2023.118200>
- Dain, Y., & Lueptow, R. (2001). Acoustic attenuation in three-component gas mixtures—Theory. *Journal of the Acoustical Society of America*, 109(5), 1955–1964. <https://doi.org/10.1121/1.1352087>
- Davy, R., Davis, J. A., Taylor, P. A., Lange, C. F., Weng, W., Whiteway, J., & Gunnlaugson, H. P. (2010). Initial analysis of air temperature and related data from the Phoenix MET station and their use in estimating turbulent heat fluxes. *Journal of Geophysical Research*, 115(E3), E00E13. <https://doi.org/10.1029/2009je003444>
- Forget, F., Hourdin, F., Fournier, R., Hourdin, C., Talagrand, O., Collins, M., et al. (1999). Improved general circulation models of the Martian atmosphere from the surface to above 80 km. *Journal of Geophysical Research: Planets*, 104(E10), 24155–24176. <https://doi.org/10.1029/1999JE001025>
- Gillier, M., & Petculescu, A. (2023). Acoustic model [Software]. *Zenodo*. <https://doi.org/10.5281/zenodo.8188828>
- Gómez-Elvira, J., Armiens, C., Carrasco, I., Genzer, M., Gómez, F., Harri, A.-M., et al. (2013). Rover environmental monitoring station. Overview of first 100 sols on Mars. In *44th annual lunar and planetary science conference* (p. 1532).
- Hagermann, A., Rosenberg, P., Towner, M., Garry, J., Svedhem, H., Leese, M., et al. (2007). Speed of sound measurements and the methane abundance in Titan's atmosphere. *Icarus*, 189(2), 538–543. <https://doi.org/10.1016/j.icarus.2007.02.004>
- Hamilton, V. E., McSweenHapke, H. Y. B. H. Y., & Hapke, B. (2005). Mineralogy of Martian atmospheric dust inferred from thermal infrared spectra of aerosols. *Journal of Geophysical Research*, 110(E12), E12006. <https://doi.org/10.1029/2005JE002501>
- Henley, D. C., & Hoidale, G. B. (1973). Attenuation and dispersion of acoustic energy by atmospheric dust. *Journal of the Acoustical Society of America*, 54(2), 437–445. <https://doi.org/10.1121/1.1913597>
- Kahre, M. A., Murphy, J. R., Newman, C. E., Wilson, R. J., Cantor, B. A., Lemmon, M. T., & Wolff, M. J. (2017). The Mars dust cycle. In *The atmosphere and climate of Mars* (Vol. 18, pp. 295–337). Cambridge University Press Cambridge. <https://doi.org/10.1017/9781139060172.010>
- Kinsler, L. E. (Ed.). (2000). *Fundamentals of acoustics* (4. ed ed.). Wiley.
- Ksanfomaliti, L., Goroshkova, N., Naraeva, M., Suvorov, A., Khondryev, V., & Yabrova, L. (1982). Acoustic measurements of the wind velocity at the Venera-13 and Venera-14 landing sites. *Soviet Astronomy Letters*, 8, 227–229.
- Lambert, J. (1977). Vibrational and rotational relaxation in gases.
- Landau, L. (1936). Theory of sound dispersion. *Physikalische Zeitschrift der Sowjetunion*, 10, 34–43.
- Leighton, T., & Petculescu, A. (2008). Sounds in space: The potential uses for acoustics in the exploration of other worlds. *Hydroacoustics*, 11, 225–239.
- Lemoine, F. G., Smith, D. E., Rowlands, D. D., Zuber, M. T., Neumann, G. A., Chinn, D. S., & Pavlis, D. E. (2001). An improved solution of the gravity field of Mars (GMM-2B) from Mars Global Surveyor. *Journal of Geophysical Research*, 106(E10), 23359–23376. <https://doi.org/10.1029/2000JE001426>
- Linstrom, P. J., & Mallard, W. G. (2023). *NIST chemistry WebBook, NIST standard reference database number 69*. National Institute of Standards and Technology. <https://doi.org/10.18434/T4D303>
- Liu, J., Richardson, M. I., & Wilson, R. (2003). An assessment of the global, seasonal, and interannual spacecraft record of Martian climate in the thermal infrared. *Journal of Geophysical Research*, 108(E8), 5089. <https://doi.org/10.1029/2002je001921>

- Lorenz, R. (2000). Compact acoustic instrumentations for studying in-situ the Martian polar CO<sub>2</sub> cycle. In *Second international conference on Mars polar science and exploration* (p. 109).
- Lorenz, R. D. (1998). Speed of sound in outer planet atmospheres. *Planetary and Space Science*, 47(1), 67–77. [https://doi.org/10.1016/S0032-0633\(98\)00099-3](https://doi.org/10.1016/S0032-0633(98)00099-3)
- Lorenz, R. D., Maurice, S., Chide, B., Mimoun, D., Stott, A., Murdoch, N., et al. (2023). The sounds of a helicopter on Mars. *Planetary and Space Science*, 230, 105684. <https://doi.org/10.1016/j.pss.2023.105684>
- Mahaffy, P. R., Webster, C. R., Atreya, S. K., Franz, H., Wong, M., Conrad, P. G., et al. (2013). Abundance and isotopic composition of gases in the Martian atmosphere from the Curiosity rover. *Science*, 341(6143), 263–266. <https://doi.org/10.1126/science.1237966>
- Maurice, S., Chide, B., Murdoch, N., Lorenz, R. D., Mimoun, D., Wiens, R. C., et al. (2022). In situ recording of Mars soundscape. *Nature*, 605(7911), 653–658. <https://doi.org/10.1038/s41586-022-04679-0>
- Millour, E., Forget, F., Spiga, A., Vals, M., Zakharov, V., & Montabone, L. (2018). Mars climate database. In *From Mars express to ExoMars*, 27–28 February 2018, Madrid, Spain.
- Mimoun, D., Cadu, A., Murdoch, N., Chide, B., Sournac, A., Parot, Y., et al. (2023). The Mars microphone onboard SuperCam. *Space Science Reviews*, 219(1), 5. <https://doi.org/10.1007/s11214-022-00945-9>
- Montmessin, F., Smith, M. D., Langevin, Y., Mellon, M. T., & Fedorova, A. (2017). The water cycle. In *The atmosphere and climate of Mars* (Vol. 18, pp. 338–373). Cambridge University Press Cambridge. <https://doi.org/10.1017/9781139060172.011>
- Munguira, A., Hueso, R., Sánchez-Lavega, A., Torre-Juarez, M. d. I., Martínez, G., Newman, C. E., et al. (2023). Near surface atmospheric temperatures at Jezero from Mars 2020 MEDA measurements. *Journal of Geophysical Research: Planets*, 128(3), e2022JE007559. <https://doi.org/10.1029/2022JE007559>
- Murdoch, N., Stott, A. E., Gillier, M., Hueso, R., Lemmon, M., Martínez, G., et al. (2022). The sound of a Martian dust devil. *Nature Communications*, 13(1), 7505. <https://doi.org/10.1038/s41467-022-35100-z>
- Petculescu, A., & Lueptow, R. (2005). Fine-tuning molecular acoustic models: Sensitivity of the predicted attenuation to the Lennard-Jones parameters. *Journal of the Acoustical Society of America*, 117(1), 175–184. <https://doi.org/10.1121/1.1828547>
- Petculescu, A., & Lueptow, R. M. (2007). Atmospheric acoustics of Titan, Mars, Venus, and Earth. *Icarus*, 186(2), 413–419. <https://doi.org/10.1016/j.icarus.2006.09.014>
- Pierce, A. D. (2019). *Acoustics: An introduction to its physical principles and applications*. Springer International Publishing. <https://doi.org/10.1007/978-3-030-11214-1>
- Poling, B. E., M. P. J., & P. O. J. (2000). *The properties of gases and liquids* (5th ed.). McGraw-Hill.
- Polkko, J., Hieta, M., Harri, A., Tamppari, L., Martínez, G., Viúdez-Moreiras, D., et al. (2023). Initial results of the relative humidity observations by MEDA instrument onboard the Mars 2020 Perseverance Rover. *Journal of Geophysical Research: Planets*, 128(2), e2022JE007447. <https://doi.org/10.1029/2022JE007447>
- Salomons, E. M. (2001). *Computational atmospheric acoustics*. Springer Netherlands. <https://doi.org/10.1007/978-94-010-0660-6>
- Sánchez-Lavega, A., del Rio-Gaztelurrutia, T., Hueso, R., Juárez, M. D. L. T., Martínez, G. M., Harri, A.-M., et al. (2023). Mars 2020 Perseverance rover studies of the Martian atmosphere over Jezero from pressure measurements. *Journal of Geophysical Research: Planets*, 128(1), e2022JE007480. <https://doi.org/10.1029/2022je007480>
- Schofield, J., Barnes, J. R., Crisp, D., Haberle, R. M., Larsen, S., Magalhaes, J., et al. (1997). The Mars Pathfinder atmospheric structure investigation/meteorology (ASI/MET) experiment. *Science*, 278(5344), 1752–1758. <https://doi.org/10.1126/science.278.5344.1752>
- Schwartz, R. N., Slawsky, Z. I., & Herzfeld, K. F. (1952). Calculation of vibrational relaxation times in gases. *The Journal of Chemical Physics*, 20(10), 1591–1599. <https://doi.org/10.1063/1.1700221>
- Sharma, R. D. (1971). Vibrational relaxation of CO<sub>2</sub> by H<sub>2</sub>O. *The Journal of Chemical Physics*, 54(2), 810–811. <https://doi.org/10.1063/1.1674916>
- Smith, M. D., Wolff, M. J., Spanovich, N., Ghosh, A., Banfield, D., Christensen, P. R., et al. (2006). One Martian year of atmospheric observations using MER Mini-TES. *Journal of Geophysical Research*, 111(E12), E12S13. <https://doi.org/10.1029/2006je002770>
- Stott, A. E., Murdoch, N., Gillier, M., Banfield, D., Bertrand, T., Chide, B., et al. (2023). Wind and turbulence observations with the Mars microphone on Perseverance. *Journal of Geophysical Research: Planets*, 128(5), e2022JE007547. <https://doi.org/10.1029/2022JE007547>
- Sutton, J. L., Leovy, C. B., & Tillman, J. E. (1978). Diurnal variations of the Martian surface layer meteorological parameters during the first 45 sols at two Viking lander sites. *Journal of the Atmospheric Sciences*, 35(12), 2346–2355. [https://doi.org/10.1175/1520-0469\(1978\)035<2346:dvtoms>2.0.co;2](https://doi.org/10.1175/1520-0469(1978)035<2346:dvtoms>2.0.co;2)
- Tanczos, F. I. (1956). Calculation of vibrational relaxation times of the chloromethanes. *The Journal of Chemical Physics*, 25(3), 439–447. <https://doi.org/10.1063/1.1742943>
- Temkin, S. (2005). *Suspension acoustics: An introduction to the physics of suspensions* (1st ed.). Cambridge University Press. <https://doi.org/10.1017/CBO9780511546129>
- Towner, M. C., Garry, J. R. C., Lorenz, R. D., Hagermann, A., Hathi, B., Svedhem, H., et al. (2006). Physical properties of Titan's surface at the Huygens landing site from the surface science package acoustic properties sensor (API-S). *Icarus*, 185(2), 457–465. <https://doi.org/10.1016/j.icarus.2006.07.013>
- Wang, H., & Richardson, M. I. (2015). The origin, evolution, and trajectory of large dust storms on Mars during Mars years 24–30 (1999–2011). *Icarus*, 251, 112–127. <https://doi.org/10.1016/j.icarus.2013.10.033>
- Widom, B., & Bauer, S. H. (1953). Energy exchange in molecular collisions. *The Journal of Chemical Physics*, 21(10), 1670–1685. <https://doi.org/10.1063/1.1698642>
- Williams, J.-P. (2001). Acoustic environment of the Martian surface. *Journal of Geophysical Research*, 106(E3), 5033–5041. <https://doi.org/10.1029/1999JE001174>
- Zou, Y., Zhu, Y., Bai, Y., Wang, L., Jia, Y., Shen, W., et al. (2021). Scientific objectives and payloads of Tianwen-1, China's first Mars exploration mission. *Advances in Space Research*, 67(2), 812–823. <https://doi.org/10.1016/j.asr.2020.11.005>
- Zuckerwar, A. J., & Meredith, R. W. (1985). Low-frequency absorption of sound in air. *Journal of the Acoustical Society of America*, 78(3), 946–955. <https://doi.org/10.1121/1.392927>